Article

Developmental Cell

BACH1 changes microglial metabolism and affects astrogenesis during mouse brain development

Graphical abstract

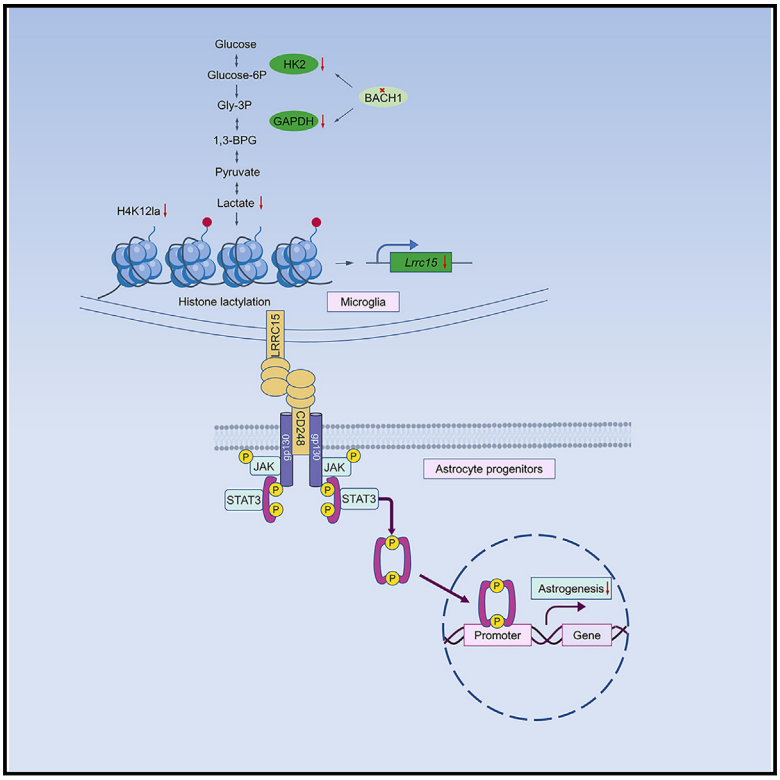

Authors

Yanyan Wang, Wenwen Wang, Libo Su, ..., Yanzhen Xie, Tianyu Zhang, Jianwei Jiao

Correspondence

jwjiao@ioz.ac.cn

In brief

Wang and Wang et al. reported that BACH1 can orchestrate astrogenesis by influencing microglia metabolic homeostasis. Absence of BACH1 leads to decreased lactate-dependent histone modification at the *Lrrc15* promoter, which affects astrogenesis through the CD248-JAK-STAT signaling pathway.

Highlights

- Transcription factor *Bach1* is essential for microglia metabolic homeostasis and histone lactylation
- Decreased H4K12la levels in microglia reduce histone lactylation enrichment at the promoter of *Lrrc15*
- Microglia-derived LRRC15 participates in astrogenesis through the JAK/STAT pathway
- Microglia *Bach1*-deficient mice show anxiety-like behavior

Wang et al., 2024, Developmental Cell *59*, 1–17
January 8, 2024
https://doi.org/10.1016/j.devcel.2023.11.018

CellPress

Developmental Cell

CellPress

Article

BACH1 changes microglial metabolism and affects astrogenesis during mouse brain development

Yanyan Wang,[1,2,3,5] Wenwen Wang,[1,4,5] Libo Su,[1,2,3] Fen Ji,[1,2,3] Mengtian Zhang,[1,2,3] Yanzhen Xie,[1,2] Tianyu Zhang,[1,2,3] and Jianwei Jiao[1,2,3,6,*]

[1]State Key Laboratory of Stem Cell and Reproductive Biology, Institute of Zoology, Chinese Academy of Sciences, Beijing 100101, China
[2]University of Chinese Academy of Sciences, Beijing 100049, China
[3]Beijing Institute for Stem Cell and Regenerative Medicine, Institute for Stem Cell and Regeneration, Chinese Academy of Sciences, Beijing 100101, China
[4]School of Life Sciences, University of Science and Technology of China, Hefei 230026, China
[5]These authors contributed equally
[6]Lead contact
*Correspondence: jwjiao@ioz.ac.cn
https://doi.org/10.1016/j.devcel.2023.11.018

SUMMARY

Microglia are highly heterogeneous as resident immune cells in the central nervous system. Although the proinflammatory phenotype of microglia is driven by the metabolic transformation in the disease state, the mechanism of metabolic reprogramming in microglia and whether it affects surrounding astrocyte progenitors have not been well elucidated. Here, we illustrate the communication between microglial metabolism and astrogenesis during embryonic development. The transcription factor BTB and CNC homology 1 (*Bach1*) reduces lactate production by inhibiting two key enzymes, HK2 and GAPDH, during glycolysis. Metabolic perturbation of microglia reduces lactate-dependent histone modification enrichment at the *Lrrc15* promoter. The microglia-derived LRRC15 interacts with CD248 to participate in the JAK/STAT pathway and influence astrogenesis. In addition, *Bach1*$^{cKO\text{-}Cx3}$ mice exhibit abnormal neuronal differentiation and anxiety-like behaviors. Altogether, this work suggests that the maintenance of microglia metabolic homeostasis during early brain development is closely related to astrogenesis, providing insights into astrogenesis and related diseases.

INTRODUCTION

Microglia originated from primitive macrophages before embryonic day (E)8.5 and entered the brain rudiment through the circulatory system. Astrocytes originate from common neural progenitor cells (NPCs) with neurons and oligodendrocytes.[1,2] During early neurogenesis, the JAK/STAT pathway of NPCs is silenced.[3,4] Then, the JAK receptor is activated, and the STAT3 dimer after phosphorylation and acetylation activates the transcription of genes associated astrogenesis.[5,6] In the context of neuroinflammation, microglia respond prior to astrocytes, and bi-directional communication between the two is more obvious. Combined with the spatial proximity of microglia and astrocyte progenitors, it is necessary to explore the relationship between microglia and astrogenesis. Secretory factors are important mediators to alter the phenotype of astrocytes, in which the form of membrane receptor-ligand communication has not been well elucidated.[7] Previous studies have shown that decreased microglial population/abnormal phagocytosis phenotypes and disturbed astrogenesis can lead to anxiety-like behaviors.[8–10] In order to accommodate and coordinate with the variational demands of the brain, microglia must undergo a series of reprogramming during development.[11] However, it is not clear whether microglia are metabolically programmed to orientate the converted requirements of the brain at different stages of neural development.

Although recent studies have mapped the transcription of microglia at different stages of development, the specific transcription factors involved in initiating metabolic reprogramming have not been clarified.[11,12] Comprehensive analysis of differentially expressed genes revealed a transcription factor, BTB and cap'n'collar (CNC) homology 1 (*Bach1*), which may be related to microglial metabolic adaptation. Well-known regulatory functions of *Bach1* include mitochondrial metabolism, glycolysis, heme homeostasis, cell cycle, and mitosis.[13–17] Most research strategies have focused on the role of *Bach1* in regulating metabolic reprogramming between oxidative phosphorylation and glycolysis.[18–20] The integrated analysis of RNA sequencing (RNA-seq) and chromatin immunoprecipitation sequencing (ChIP-seq) in lung cancer cells found that *Bach1* activated its

Please cite this article in press as: Wang et al., BACH1 changes microglial metabolism and affects astrogenesis during mouse brain development, Developmental Cell (2023), https://doi.org/10.1016/j.devcel.2023.11.018

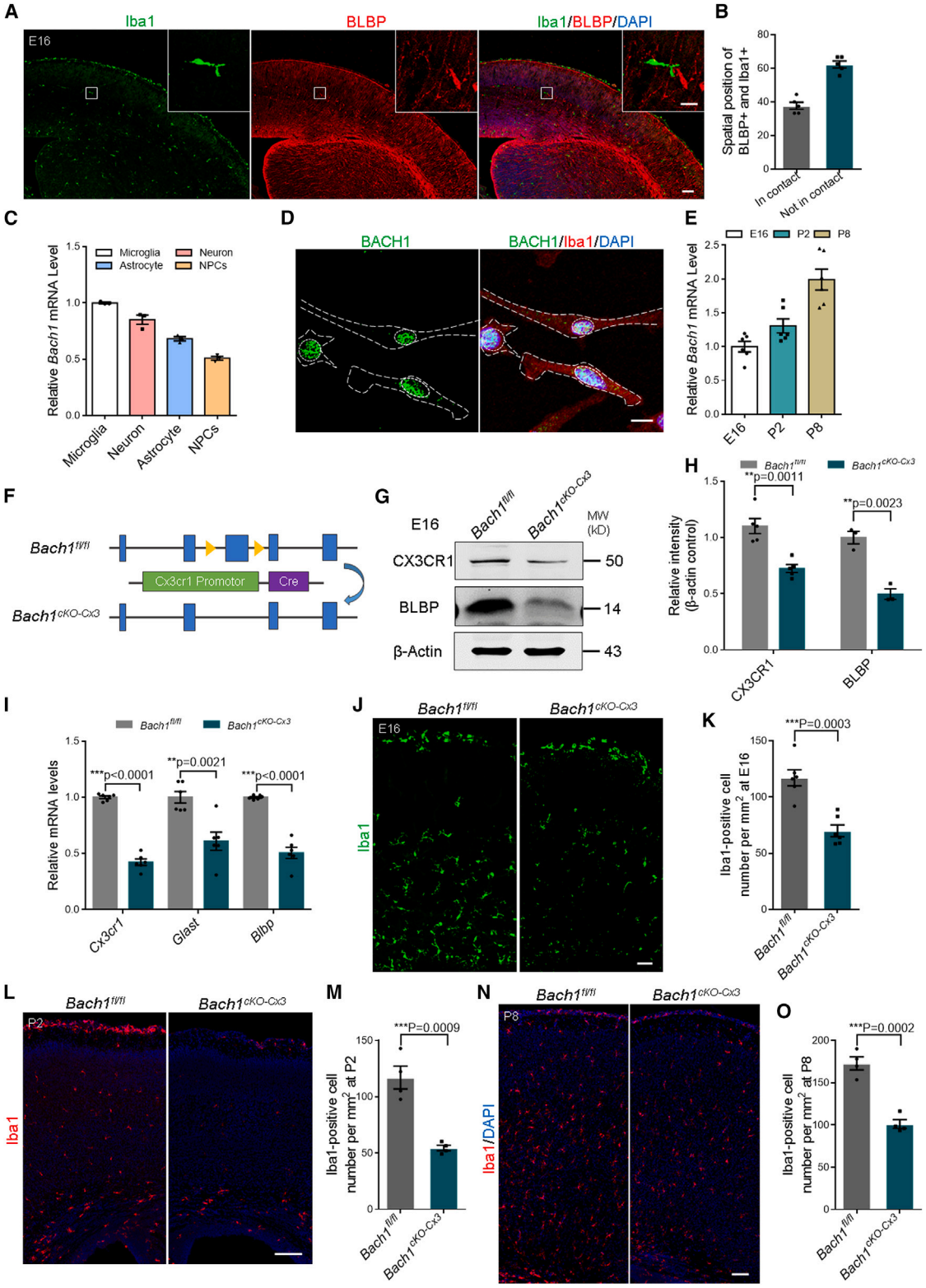

Figure 1. Microglia contact neighboring astrocyte progenitors, and BACH1 deficiency disrupts the microglial populations

(A) Immunofluorescence staining of Iba1 and BLBP in the E16 brain cortices. Scale bars, 50 μm; for zoom, 20 μm.

(B) Quantification of contact percentage between BLBP+ and Iba1+ at E16 (n = 5 mice per group).

(C) Quantitative real-time PCR monitoring expression of *Bach1* in microglia, neurons, astrocytes, and NPCs (n = 3 mice per group).

(D) Confocal immunofluorescence image of BACH1 and Iba1 in microglia showing the cell localization. Scale bars, 10 μm.

(legend continued on next page)

Please cite this article in press as: Wang et al., BACH1 changes microglial metabolism and affects astrogenesis during mouse brain development, Developmental Cell (2023), https://doi.org/10.1016/j.devcel.2023.11.018

transcription at the promoter of hexokinase 2 (*Hk2*) and glyceraldehyde 3-phosphate dehydrogenase (*Gapdh*) to regulate glucose consumption and lactate production.[16] More recently, lactate produced by glycolysis has been considered a substrate for histone lactylation, and histone lactylation modification has demonstrated an interesting function of stimulating gene transcription.[21–23] As an important governor in the regulation of glycolysis, it is particularly exciting to explore the function of *Bach1* in the metabolic programming of developing microglia.

In this study, we show that the absence of *Bach1* in microglia reduces lactate production by restricting the transcription of *Hk2* and *Gapdh*. Among these predicted histone lactylation binding sites, the significant reduction of H4K12la sites is interesting. We find that *Lrrc15* plays a crucial role in the communication between microglia and astrocyte progenitors. Taken together, our work elucidated that metabolic perturbations of *Bach1*-deficient microglia cause decreased lactate modification of downstream target *Lrrc15* at the HK412la site. We identified microglia-astrocyte communication mediated by the LRRC15-CD248-JAK/STAT3 axis and induced anxiety-like behavior in $Bach1^{cKO\text{-}Cx3}$ mice, supporting the microglial metabolic adaptation and microglia-astrocyte communication during early brain development and having important implications for gliogenesis and related diseases.

RESULTS

The developing microglia are related to astrocyte progenitors in the cortex

In the intricate course of early brain development, microglia closely interact with astrocyte progenitors and act as an important component of the neuroglia niche by physical proximity.[24,25] Therefore, we evaluated the positional relationship between microglia and astrocyte progenitors at E16. Coimmunostaining and quantitative analyses revealed that 38% of BLBP+ astrocyte precursors were physically close to Iba1+ microglia (Figures 1A and 1B). Furthermore, the transgenic reporter line CX3CR1-GFP revealed that CX3CR1+ microglia were colonized near glial progenitors (glutamate and aspartate transporter [GLAST]) at E16 (Figures S1A and S1B). *Bach1* is a member of the CNC b-Zip family that regulates core genes involved in the central carbon metabolic pathways of cancer cells.[26] During embryonic development, various cell types maintain the homeostasis of the central nervous system (CNS) by adjusting the metabolic state.[27–29] To inquire the role of *Bach1* in the developing cerebral cortex, we analyzed the expression levels of *Bach1* in microglia, neurons, astrocytes, and NPCs. The results exhibited that *Bach1* was highly expressed in microglia than other cell types (Figure 1C). Moreover, immunostaining assays clearly exhibited that BACH1 was richly expressed in primary Iba1+ microglia (Figure 1D). Then, we found that the relative mRNA levels of *Bach1* in flow-sorted microglia were gradually increased with the progression of astrogenesis from E16 to postnatal day 8 (P8) (Figure 1E). Taken together, these results show that *Bach1* was positively correlated with developing microglia, and the spatial and temporal expression patterns strongly suggest that *Bach1* was involved in the communication between microglia and astrocytes during brain development.

BACH1 deletion in microglia reduces microglia and astrocyte precursor population

To further investigate the function of microglial *Bach1* in the early brain, *Cx3cr1*-Cre mice were crossed with $Bach1^{fl/fl}$ mice to generate microglial *Bach1* conditional knockout mice ($Bach1^{cKO\text{-}Cx3}$) (Figure 1F). First, microglia were isolated by FACS at E16 and cultured for western blotting. The results reveal that the expression of BACH1 was specifically reduced in $Bach1^{cKO\text{-}Cx3}$ microglia (Figures S1C and S1D). Then, quantitative real-time PCR detection of purified microglia displayed that the abundance of *Bach1* mRNA was greatly reduced (Figure S1E). Furthermore, BACH1 and Iba1 were co-immunostained with purified microglia from $Bach1^{fl/fl}$ and $Bach1^{cKO\text{-}Cx3}$ cortices. The results confirmed that *Bach1* expression was significantly decreased (Figures S1F and S1G). Then, we explored the phenotypes of the $Bach1^{cKO\text{-}Cx3}$ mice. The expression of CX3CR1 in $Bach1^{cKO\text{-}Cx3}$ mice was significantly reduced at E16. Interestingly, we were surprised to find that BLBP was significantly reduced in E16 $Bach1^{cKO\text{-}Cx3}$ mice (Figures 1G and 1H). Furthermore, real-time PCR analysis of the cerebral cortex at E16 confirmed the decreased abundance of *Cx3cr1*, *Glast*, and *Blbp* mRNA in $Bach1^{cKO\text{-}Cx3}$ mice (Figure 1I). To further explore the impact of microglia-derived *Bach1* on astrocytic differentiation in the early brain, we next observed Iba1+ microglia populations of different astrogenesis milestones in $Bach1^{fl/fl}$ and $Bach1^{cKO\text{-}Cx3}$ cerebral cortices. These data demonstrate that knocking out *Bach1* in microglia afflicted the production of Iba1+ microglia at E16 when astrogenesis started in fetal brain (Figures 1J and 1K). Furthermore, our results exhibit a dramatic reduction of microglia in *Bach1*-deleted cerebral cortices at the peak and end of astrogenesis (Figures 1L–1O).

(E) Quantitative real-time PCR monitoring expression of *Bach1* in flow-sorted microglia at E16, P2, and P8 (n = 6 mice per group).
(F) Schematic diagram of constructing *Bach1* conditional knockout mice in microglia.
(G and H) The protein levels of CX3CR1 and BLBP in $Bach1^{fl/fl}$ and $Bach1^{cKO\text{-}Cx3}$ cerebral cortex at E16 were detected (G) and quantified (H) by western blotting (for CX3CR1, n = 5; for BLBP, n = 3).
(I) Quantitative real-time PCR assays monitoring the expression of *Cx3cr1*, *Glast*, and *Blbp* in $Bach1^{fl/fl}$ and $Bach1^{cKO\text{-}Cx3}$ cerebral cortex at E16 (n = 6 mice per group).
(J) Immunofluorescence staining of Iba1 in $Bach1^{fl/fl}$ and $Bach1^{cKO\text{-}Cx3}$ cerebral cortex at E16. Scale bars, 50 μm.
(K) Quantification showing the decreased number of Iba1+ cells in $Bach1^{cKO\text{-}Cx3}$ mice at E16 (n = 6 mice per group).
(L) Confocal immunofluorescence image of Iba1 staining in $Bach1^{fl/fl}$ and $Bach1^{cKO\text{-}Cx3}$ cerebral cortex at P2. Scale bars, 100 μm.
(M) Quantification showing the decreased number of Iba1+ cells in $Bach1^{cKO\text{-}Cx3}$ mice at P2 (n = 4 mice per group).
(N) Immunofluorescence staining of Iba1 in $Bach1^{fl/fl}$ and $Bach1^{cKO\text{-}Cx3}$ cerebral cortex at P8. Scale bars, 100 μm.
(O) Quantitative analysis showed that Iba1+ cells in $Bach1^{cKO\text{-}Cx3}$ mice at P8 were continuously reduced (n = 4 mice per group).
All data are presented as the mean ± SEM. Unpaired two-tailed Student's t test or one-way ANOVA; *p < 0.05, **p < 0.01, ***p < 0.001, ****p < 0.0001, n.s., not significant.
See also Figure S1.

Please cite this article in press as: Wang et al., BACH1 changes microglial metabolism and affects astrogenesis during mouse brain development, Developmental Cell (2023), https://doi.org/10.1016/j.devcel.2023.11.018

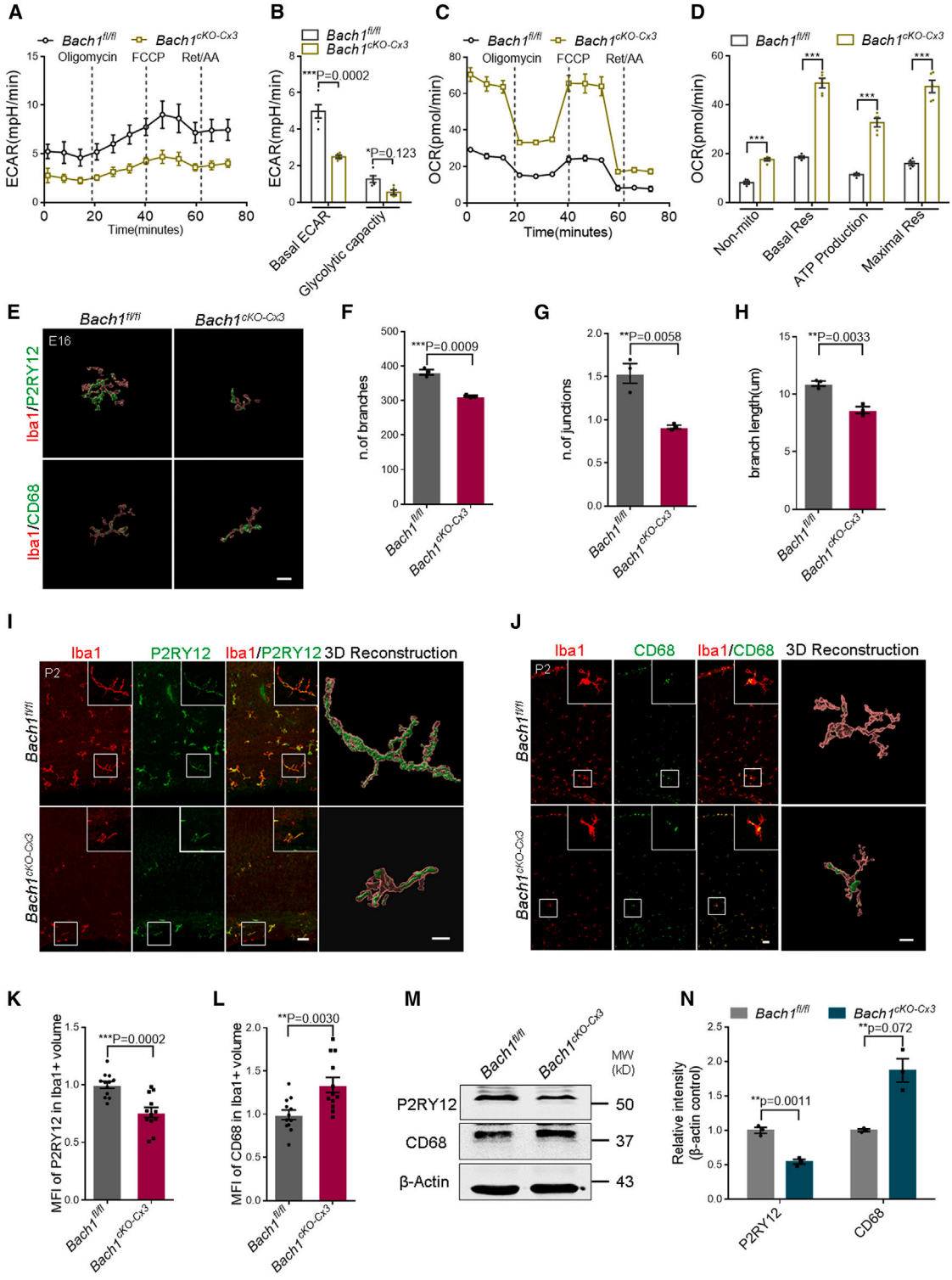

Figure 2. The absence of BACH1 alters microglial metabolic patterns and disrupts homeostasis

(A) ECAR traces of flow-sorted *Bach1*$^{fl/fl}$ and *Bach1*$^{cKO\text{-}Cx3}$ microglia were obtained using a Seahorse XF96 Analyzer.

(B) Statistical analyses of basal ECAR and glycolytic capacity (n = 5 mice per group).

(C) OCR traces of flow-sorted *Bach1*$^{fl/fl}$ and *Bach1*$^{cKO\text{-}Cx3}$ microglia were analyzed by Mito Stress test assay.

(D) Statistical analyses of non-mitochondrial respiration, basal respiration, ATP production, and maximal respiration (n = 5 mice per group).

(E) Representative 3D reconstruction images of Iba1 co-stained with P2RY12 or CD68 in the cerebral cortex of *Bach1*$^{fl/fl}$ and *Bach1*$^{cKO\text{-}Cx3}$ mice at E16. Scale bars, 20 μm.

(legend continued on next page)

Please cite this article in press as: Wang et al., BACH1 changes microglial metabolism and affects astrogenesis during mouse brain development, Developmental Cell (2023), https://doi.org/10.1016/j.devcel.2023.11.018

We performed immunofluorescence staining for Iba1 and BACH1 on *Bach1*$^{fl/fl}$ and *Bach1*$^{cKO\text{-}Cx3}$ mice brains at E16, and the results presented a dramatic reduction in the number of BACH1+ microglia in *Bach1*$^{cKO\text{-}Cx3}$ cerebral cortex (Figures S1H and S1I). Meanwhile, locally enlarged stack confocal images showed the nuclear localization of BACH1 in IBA1+ microglia (Figure S1J). In addition, we also examined the production of oligodendrocyte lineage cells. Western blotting displayed that the protein levels of the oligodendrocyte markers MBP and OLIG2 were not significantly changed in *Bach1*$^{cKO\text{-}Cx3}$ mice (Figures S1K and S1L). Immunofluorescence staining was consistent with the results (Figures S1M and S1N). To explore the effects of apoptosis in *Bach1*$^{cKO\text{-}Cx3}$ mice, immunofluorescence staining was performed by labeling the apoptosis marker cleaved caspase3. There was no significant difference in apoptosis between *Bach1*$^{fl/fl}$ and *Bach1*$^{cKO\text{-}Cx3}$ brain cortices, indicating that the reduction of microglia and astrocyte precursors in the *Bach1*$^{cKO\text{-}Cx3}$ brain was not caused by apoptosis (Figures S1O and S1P). In summary, our studies show that microglial *Bach1* inactivation generates abnormal development of microglia and astrocytes.

The absence of BACH1 alters microglial metabolic patterns and disrupts the homeostasis state

Bach1 is known to be involved in the regulation of various physiological processes, and recent studies have found that BACH1 plays a role in regulating the metabolic pathways of cancer cells.[26] However, it is unclear whether *Bach1* plays a role in microglial metabolic transitions during early cortical development. Here, we isolated *Bach1*$^{cKO\text{-}Cx3}$ microglia by flow cytometry and assessed metabolic phenotypes by measuring both oxygen consumption rate (OCR) and extra cellular acidification rate (ECAR). The results showed that *Bach1*$^{cKO\text{-}Cx3}$ microglia displayed increased basal as well as maximum OCR but decreased ECAR (Figures 2A–2D). We also confirmed by tetramethylrhodamine ethyl ester perchlorate (TMRE) that the mitochondrial membrane potential of *Bach1*-deficient microglia was significantly increased (Figures S2A and S2B). Through the cell-permeant MitoTracker probes visualization mitochondria, we found that the length, volume, average branch, and number of branch junctions of mitochondria in *Bach1*$^{cKO\text{-}Cx3}$ microglia increased to varying degrees, indicating that the mitochondrial dynamics of *Bach1*-deficient microglia were enhanced (Figures S2C–S2G). These results indicated that *Bach1* plays a core role in deciding the metabolic patterns of microglia during early cortical development.

Considering the correlation between microglial metabolic remodeling and homeostasis, we performed immunofluorescence staining for Iba1, P2RY12 (homeostatic microglial marker), and CD68 (a marker for activated microglia) on *Bach1*$^{fl/fl}$ and *Bach1*$^{cKO\text{-}Cx3}$ mice brains at E16, and the three-dimensional (3D) reconstruction was performed (Figure 2E). Unbiased morphological analysis of the number of branches, the number of junctions, and the branch length revealed gross morphological defects of *Bach1*$^{cKO\text{-}Cx3}$ microglia (Figures 2F–2H). We also performed immunofluorescence staining for Iba1, P2RY12, and CD68 in cerebral cortex sections of *Bach1*$^{fl/fl}$ and *Bach1*$^{cKO\text{-}Cx3}$ mice during the peak period of astrogenesis (Figures 2I and 2J). The immunofluorescence intensity (MFI) of P2RY12 and CD68 in Iba1+ volume was analyzed, respectively. We found that the MFI of P2RY12 in iba1+ volume of *Bach1*$^{cKO\text{-}Cx3}$ mice was decreased and that of CD68 was increased (Figures 2K and 2L). In addition, we also found consistent results through western blotting (Figures 2M and 2N). Furthermore, real-time PCR analysis of the cerebral cortex at E18 showed that mRNA levels of resting microglia markers *Cx3cr1*, *Tmem119*, and astrocyte progenitors marker *Blbp* decreased, whereas *Apoe* levels of dysregulated microglia increased in *Bach1*$^{cKO\text{-}Cx3}$ mice, indicating homeostasis imbalance in *Bach1*-deficient microglia (Figure S2H). We stained Iba1 with P2RY12 or CD68 and found that this difference persisted in the adult brain (Figures S2I–S2M). Global and locally enlarged stack images showed that the MFI of P2RY12 in BACH1-negative microglia of *Bach1*$^{cKO\text{-}Cx3}$ mice was generally reduced, which proved that the reduction of P2RY12 occurred in microglia that in fact lost BACH1 (Figures S2N–S2P). These results indicate that microglia-derived BACH1 activity is essential for suitable metabolism and homeostasis during cortical development.

Disrupted microglial metabolism caused by BACH1 leads to a persistent decrease in astrocyte generation during brain development

To investigate the changes of astrogenesis in *Bach1*$^{cKO\text{-}Cx3}$ mice, immunofluorescence staining of S100β/GFAP was performed at P2, and the data showed that the number of S100β+ or GFAP+ astrocytes in *Bach1*$^{cKO\text{-}Cx3}$ mice was significantly reduced (Figures 3A–3D). The results of immunofluorescence staining and western blotting showed that the number of GFAP+ astrocytes in *Bach1*$^{cKO\text{-}Cx3}$ brains at P8 continued to decrease (Figures 3E, 3F, S3A, and S3B). This developmental defect in astrocytes can be detected until P60 (Figures S3C–S3F). We electroporated a GFP expression vector at E15.5 and harvested sections 4 days later to evaluate the proportion of transfected cells co-expressing BLBP. It was found that 9% of the transfected cells expressed BLBP in *Bach1*$^{fl/fl}$ mice and only 4.5% in *Bach1*$^{cKO\text{-}Cx3}$ mice (Figures 3G and 3H). Then, we

(F–H) Quantitative analysis showed the number of branches (F), the number of junctions (G), and the branch length (H) in *Bach1*$^{fl/fl}$ and *Bach1*$^{cKO\text{-}Cx3}$ microglia (n = 3 mice per group).

(I and J) Confocal immunofluorescence and representative 3D reconstruction image of Iba1 co-stained with P2RY12 (I) or CD68 (J) in the cerebral cortex of *Bach1*$^{fl/fl}$ and *Bach1*$^{cKO\text{-}Cx3}$ mice at P2. Scale bars, 50 μm; for zoom, 10 μm.

(K and L) Quantification of the MFI of P2RY12 (K) or CD68 (L) in Iba1+ microglia (n = 12 cells per group).

(M and N) The protein levels of P2RY12 and CD68 in *Bach1*$^{fl/fl}$ and *Bach1*$^{cKO\text{-}Cx3}$ cerebral cortex at E16 were detected (M) and quantified (N) by western blotting (n = 3 mice per group).

All data are presented as the mean ± SEM. Unpaired two-tailed Student's t test or one-way ANOVA; *p < 0.05, **p < 0.01, ***p < 0.001, ****p < 0.0001, n.s., not significant.

See also Figure S2.

Please cite this article in press as: Wang et al., BACH1 changes microglial metabolism and affects astrogenesis during mouse brain development, Developmental Cell (2023), https://doi.org/10.1016/j.devcel.2023.11.018

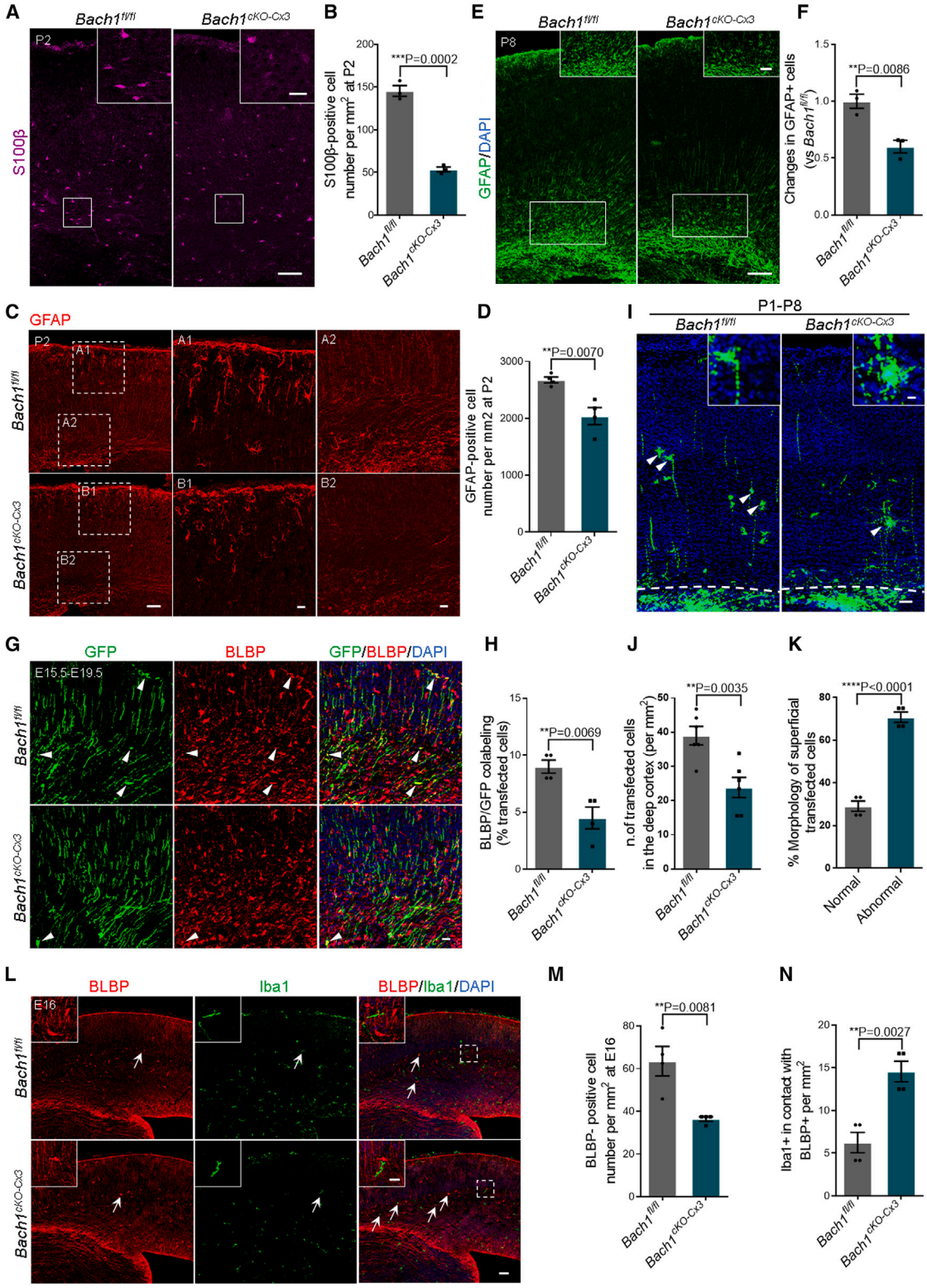

Figure 3. Astrogenesis is impaired in response to microglial metabolism disorder during brain development

(A) Confocal immunofluorescence image of S100β+ cells in *Bach1*$^{fl/fl}$ and *Bach1*$^{cKO\text{-}Cx3}$ cerebral cortex at P2. The box in the upper right shows regions of higher magnification. Scale bars, 100 μm; for zoom, 20 μm.

(B) Quantification showing the decreased number of S100β+ cells in *Bach1*$^{cKO\text{-}Cx3}$ mice at P2 (n = 3 mice per group).

(legend continued on next page)

Please cite this article in press as: Wang et al., BACH1 changes microglial metabolism and affects astrogenesis during mouse brain development, Developmental Cell (2023), https://doi.org/10.1016/j.devcel.2023.11.018

electroporated a GFP expression vector at P1 and measured development progress at P8. Compared with *Bach1*$^{fl/fl}$ mice, the migration of mature astrocytes to the deep cortex of *Bach1*$^{cKO\text{-}Cx3}$ mice was reduced, the morphology of astrocytes was unclear, and 71% of superficial transfected cells showed abnormal morphology (Figures 3I–3K). Subsequently, immunostaining showed that the contact between Iba1+ and BLBP+ cells in *Bach1*$^{cKO\text{-}Cx3}$ mice increased significantly and the number of BLBP+ astrocyte progenitors decreased (Figures 3L–3N).

The above results indicate that the lack of *Bach1* in microglia leads to abnormal astrogenesis, which makes us curious about the effect of astrogenic *Bach1* on their own development. Therefore, we constructed *Bach1* knockdown plasmid and tested the knockout efficiency (Figures S3G and S3H). Subsequently, *Bach1*-shRNA plasmids were electrically transferred into the lateral ventricles of E16 embryos, and the cerebral cortex was harvested at P2 (Figure S3I). The proportion of GFAP+ cells in GFP+ cells was evaluated, and no significant change was found between *Bach1*-shRNA and control groups (Figures S3J and S3K). Then, we generated *Bach1*$^{cKO\text{-}Gfap}$ conditional knockout mice (Figure S3L). Similar to the results of *Bach1*-shRNA, there was no significant decrease in the number of BLBP+ cells between *Bach1*$^{fl/fl}$ and *Bach1*$^{cKO\text{-}Gfap}$ mice (Figures S3M and S3N). In addition, we detected the expressions of GFAP and ALDH1L1 at P8. The results exhibited that there was no obvious change in the expression level of ALDH1L1 and GFAP compared with *Bach1*$^{fl/fl}$ mice (Figures S3O and S3P). Together, these results showed that *Bach1*$^{cKO\text{-}Cx3}$ mice had impaired astrogenesis, whereas *Bach1*$^{cKO\text{-}Gfap}$ mice had no significant effect on astrogenesis.

Lentivirus and AAV-mediated BACH1 knockdown of microglia *in vivo* and *in vitro* showed similar gliogenesis disorders as *Bach1*$^{cKO\text{-}Cx3}$ mice

To further determine the effect of BACH1 deletion in microglia, we transduced primary microglia with lentivirus for about 24 h. Immunofluorescence staining results exhibited that the percentage of GFP+Iba1+/Iba1+ reached 80% (Figures S4A and S4B). We found that the expression level of BACH1 was markedly decreased in the pSicoR-GFP-sh*Bach1* group (Figures S4C and S4D). Subsequently, we found that the MFI of CD68 in Iba1+ volume increased significantly in the sh*Bach1* group (Figures 4A and 4B). We co-cultured glial progenitors with microglia infected with sh*Bach1* lentivirus and evaluated the proportion of BLBP+ and GFAP+ cells. The results showed that the percentage of BLBP+ and GFAP+ cells decreased in the sh*Bach1* group (Figures 4C and 4D).

Bach1 knockdown in microglia-dominated macrophages driven by the F4/80 promoter was achieved by adeno-associated virus (AAV). First, AAV-F4/80-sh*Bach1*-GFP was injected into the lateral ventricles of E13.5 embryos, and AAV-F4/80-NCshRNA-GFP was used as control (Figure S4E). 2 weeks later, immunofluorescence staining showed that the percentage of GFP+Iba1+/Iba1+ reached 71% (Figures S4F and S4G). In addition, we found that the expression level of BACH1 decreased dramatically in the AAV-F4/80-sh*Bach1*-GFP group (Figures S4H and S4I). Subsequently, Iba1 and P2RY12/CD68 co-staining showed abnormal microglial homeostasis (Figures 4E–4H). Similarly, the number of GFAP+ and S100β+ astrocytes in the cerebral cortex of the AAV-F4/80-sh*Bach1*-GFP group was reduced (Figures 4I–4L). Taken together, these evidences enrich the approach of knockdown BACH1 in microglia and make the effect of BACH1 loss in microglia more solid.

Dysmetabolism of microglia impairs the proliferation and differentiation of NPCs during cortical development

Previous studies have shown that microglial disorders impair neurogenesis during cortical development.[30–32] To investigate this hypothesis, immunofluorescence staining of Pax6/Sox2 was performed at E13.5, and the results presented that the number of Pax6+/Sox2 NPCs in *Bach1*$^{cKO\text{-}Cx3}$ mice was reduced (Figures S5A–S5D). We quantified the number of wide widespread neurons in the E16 mutant cortex by immunofluorescence staining Tuj1, which showed that microglia metabolic disorders led to a reduction in the number of neurons (Figures S5E and S5F). Consistently, similar results were obtained by western blotting of NeuN and Tuj1 protein levels (Figures S5G and S5H). Then, we found that the number of Satb2+ and

(C) Immunofluorescence staining of GFAP in *Bach1*$^{fl/fl}$ and *Bach1*$^{cKO\text{-}Cx3}$ mice brain section at P2. A1, A2, B1, and B2 are higher-magnification images. Scale bars, 100 μm; for zoom, 20 μm.
(D) Quantification showing the decreased number of GFAP+ cells in *Bach1*$^{cKO\text{-}Cx3}$ mice at P2 (n = 4 mice per group).
(E) Confocal immunofluorescence image of GFAP+ cells in *Bach1*$^{fl/fl}$ and *Bach1*$^{cKO\text{-}Cx3}$ cerebral cortex at P8. The box in the upper right show regions of higher magnification. Scale bars, 100 μm; for zoom, 50 μm.
(F) Quantitative analysis showed that GFAP+ cells in *Bach1*$^{cKO\text{-}Cx3}$ mice at P8 were continuously reduced (n = 3 mice per group).
(G) GFP was electroporated into E15.5 embryonic mice brains, and the brains were harvested at E19.5 for BLBP immunostaining. Scale bars, 20 μm.
(H) Quantitative analysis showed that the proportion of the transfected cells co-expressing BLBP was decreased in *Bach1*$^{cKO\text{-}Cx3}$ cerebral cortex (n = 4 mice per group).
(I) GFP was electrocuted into P1 newborn mice brain, and brain sections were harvested at P8. Confocal images showing the abnormal morphology of GFP-expressing astrocytes in *Bach1*$^{cKO\text{-}Cx3}$ mice at p8 (arrowhead). Scale bars, 50 μm; for zoom, 10 μm.
(J) Quantification of the number of deep transfected cells in *Bach1*$^{fl/fl}$ and *Bach1*$^{cKO\text{-}Cx3}$ mice brains (n = 6 mice per group).
(K) Quantification of the morphology of superficial transfected cells in *Bach1*$^{cKO\text{-}Cx3}$ mice brains (n = 4 mice per group).
(L) Immunofluorescence staining of BLBP and Iba1 in *Bach1*$^{fl/fl}$ and *Bach1*$^{cKO\text{-}Cx3}$ mice at E16. The box in the upper left shows regions of higher magnification. Scale bars, 50 μm; for zoom, 10 μm.
(M) Quantification showing the decreased number of BLBP+ cells in *Bach1*$^{cKO\text{-}Cx3}$ mice at E16 (n = 4 mice per group).
(N) Statistical analysis of contact between Iba1+ microglia and BLBP+ astrocyte progenitors per mm^2. Contact was defined as an Iba1+ cell overlapping a BLBP+ cell or a distance less than or equal to 2 μm (n = 4 mice per group).
All data are presented as the mean ± SEM. Unpaired two-tailed Student's t test or one-way ANOVA; *p < 0.05, **p < 0.01, ***p < 0.001, ****p < 0.0001, n.s., not significant.
See also Figure S3.

Please cite this article in press as: Wang et al., BACH1 changes microglial metabolism and affects astrogenesis during mouse brain development, Developmental Cell (2023), https://doi.org/10.1016/j.devcel.2023.11.018

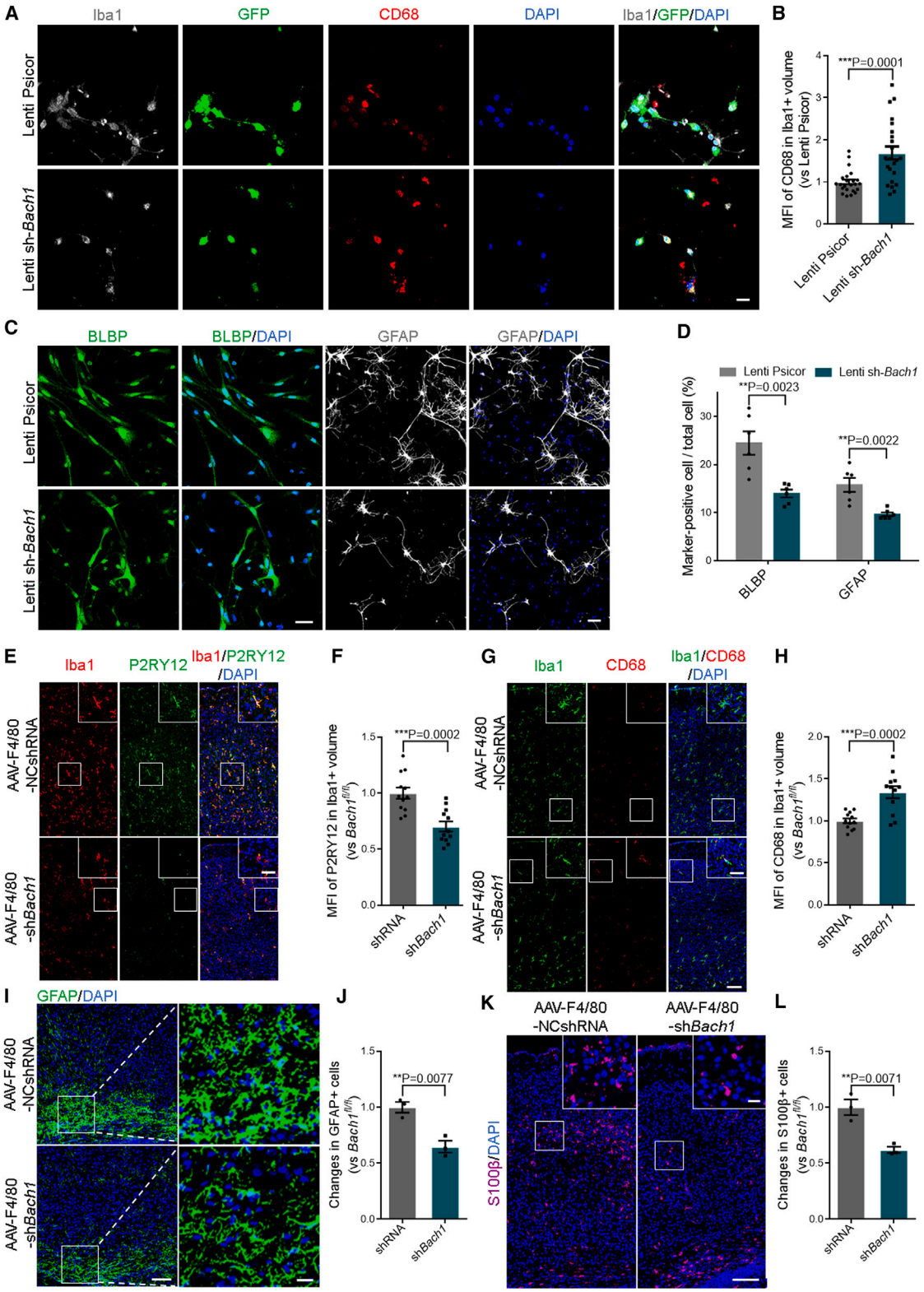

Figure 4. Lentivirus and AAV-mediated microglial BACH1 knockdown impairs microglial homeostasis and astrogenesis

(A) Immunofluorescence of Iba1 and CD68 in primary microglia transfected with pSicoR-GFP or pSicoR-GFP-sh*Bach1* for 2 days. Scale bars, 20 μm.

(B) Quantification of the MFI of CD68 in Iba1+ cells (n = 23 cells per group).

(legend continued on next page)

Please cite this article in press as: Wang et al., BACH1 changes microglial metabolism and affects astrogenesis during mouse brain development, Developmental Cell (2023), https://doi.org/10.1016/j.devcel.2023.11.018

Tbr1+ upper-layer neurons in the mutant cortex was reduced (Figures S5I and S5J). This abnormal neuronal differentiation in *Bach1*$^{cKO\text{-}Cx3}$ mice sparked our interest in exploring neuronal morphology. Therefore, we electroporated the GFP plasmids into the lateral ventricles of E13.5 embryos and harvested them at P15. We found that primary dendrites and total dendritic lengths of GFP+ neurons tracked in the cortex of *Bach1*$^{cKO\text{-}Cx3}$ mice were reduced (Figures S5K–S5M). These results demonstrated that microglia-derived BACH1 is necessary for the proliferation and differentiation of NPCs and the morphology of neurons during cortical development.

Loss of BACH1 contributes to anxiety-like behavior in pup and adult mice

Prior to all behavioral experiments, motor ability and balance were first measured, which showed no significant differences in grip strength and latency to fall between *Bach1*$^{fl/fl}$ and *Bach1*$^{cKO\text{-}Cx3}$ mice (Figures S6A and S6B). First, *Bach1*$^{cKO\text{-}Cx3}$ mice and their littermates, *Bach1*$^{fl/fl}$ mice, were analyzed in an open-field test (Figure 5A). *Bach1*$^{cKO\text{-}Cx3}$ mice showed no significant difference in the traveled distance but stayed in the central region for a short time (Figures 5B and 5C). The elevated-plus maze results presented that the *Bach1*$^{cKO\text{-}Cx3}$ mice spent more time in the closed arm and less time in the open arm, indicating increased anxiety in the mutant mice (Figures 5D–5F). Then, the Y-maze test exhibited that microglial *Bach1* deficiency did not lead to depressive-like forms and working memory deficit (Figures S6C and S6D).

Then, to explore whether *Bach1*$^{cKO\text{-}Cx3}$ mice have social interaction deficits, we conducted a three-chamber social interaction experiment (Figure 5G). Compared with the empty cage, *Bach1*$^{fl/fl}$ mice showed great interest in the chamber where a novel stranger mouse (stranger 1) was placed, whereas *Bach1*$^{cKO\text{-}Cx3}$ mice showed no significant interest (Figure 5H). When the stranger 2 mouse was placed into the empty cage, *Bach1*$^{cKO\text{-}Cx3}$ mice showed no significant preference for stranger 2 mice (Figure 5I). Based on the above behavioral phenotype in *Bach1*$^{cKO\text{-}Cx3}$ mice, we speculate that the absence of *Bach1* in microglia may cause anxiety-like behavior. To test this hypothesis, we executed an ultrasonic vocalization (USV) experiment at P8 (Figure 5J). *Bach1*$^{cKO\text{-}Cx3}$ mice exhibited shorter call durations and fewer calls (Figures 5K and 5L). Marble-burying test exhibited that *Bach1*$^{cKO\text{-}Cx3}$ mice were more inclined to dig (Figures S6E and S6F). Taken together, these evidences indicate that *Bach1*$^{cKO\text{-}Cx3}$ mice exhibited anxiety-like behaviors. In addition, we administered PLX5622 to the embryonic lateral ventricles every other day from E13 to P0. After birth, P0 pups were treated with PLX5622 intraperitoneally daily until P7 (Figure S6G and Video S1). Immunofluorescence staining showed effective ablation of Iba1+ microglia and a decrease in the number of GFAP+ astrocytes (Figures S6H–S6J). Immunostaining showed a decrease in the number of upper-layer neurons of PLX5622-treated cortex (Figures S6K and S6L). Finally, we executed the USV experiment at P8 and found that the pups treated with PLX5622 showed less duration and frequency of calls (Figures S6M–S6O).

BACH1 regulates astrogenesis by targeting LRRC15 in microglia

Studies have shown that *Bach1* is involved in the expression of key enzymes in the aerobic glycolysis pathway in cancer cells (Figure 6A). We found that *Bach1* was dramatically enriched in the *Hk2* and *Gapdh* promoter region in glial cells by ChIP assay (Figures 6B and 6C). In addition, colorimetric analysis showed that the lactate level of *Bach1*$^{cKO\text{-}Cx3}$ mice was observably lower than that of *Bach1*$^{fl/fl}$ mice (Figure S7A). Since lactate is a precursor that stimulates histone lactylation, we detected lactate modifications and found that H4K12la levels in *Bach1*-deleted microglia were dramatically reduced (Figures 6D and 6E). Immunofluorescence analysis confirmed this finding (Figures 6F and 6G). We injected lactate into the embryonic lateral ventricle at E13.5 and again at E16. Subsequently, USV tests were performed at P8, and the results showed that the increase in lactate during brain development could rescue behavioral abnormalities in *Bach1*$^{cKO\text{-}Cx3}$ mice (Figures S7B–S7D).

The alteration of histone modification can affect the transcriptional activation and inhibition of target genes.[23] To explore the downstream mechanism of *Bach1*, we isolated CD45+CD11b+ cells from the cerebral cortex of E16 *Bach1*$^{cKO\text{-}Cx3}$ mice and littermate *Bach1*$^{fl/fl}$ mice by flow cytometry and performed RNA transcriptomic sequencing (Figures S7E and S7F).

(C) Immunofluorescence staining of astrocyte progenitors co-cultured with microglia transduced with lentivirus for 24 h. Cells co-cultured for 2 days were stained with BLBP, and cells co-cultured for 5 days were stained with GFAP. Scale bars, 50 μm.
(D) Quantify the number of BLBP+ and GFAP+ cells in systems co-cultured with lentivirus transducing microglia (n = 6 independent experiments).
(E) Confocal immunofluorescence of Iba1 co-stained with P2RY12 in the cerebral cortex after 2 weeks of AAV injection. Scale bars, 100 μm; for zoom, 50 μm.
(F) Quantification of the MFI of P2RY12 in Iba1+ microglia (n = 12 cells per group).
(G) Confocal immunofluorescence of Iba1 co-stained with CD68 in the cerebral cortex after 2 weeks of AAV injection. Scale bars, 100 μm; for zoom, 50 μm.
(H) Quantification of the MFI of CD68 in Iba1+ microglia (n = 12 cells per group).
(I) Immunofluorescence staining of GFAP in the cerebral cortex after 2 weeks of AAV injection. The box in the right shows regions of higher magnification. Scale bars, 100 μm; for zoom, 20 μm.
(J) Quantitative analysis showed that the number of GFAP+ cells decreased in the brain sections of mice injected with AAV-F4/80-sh*Bach1*-GFP group (n = 3 mice per group).
(K) Confocal immunofluorescence image of S100β in the cerebral cortex after 2 weeks of AAV injection. The box in the upper right shows regions of higher magnification. Scale bars, 100 μm; for zoom, 20 μm.
(L) Quantification showing the decreased number of S100β+ cells in the brain sections of mice injected with AAV-F4/80-sh*Bach1*-GFP group (n = 3 mice per group).
All data are presented as the mean ± SEM. Unpaired two-tailed Student's t test or one-way ANOVA; *p < 0.05, **p < 0.01, ***p < 0.001, ****p < 0.0001, n.s., not significant.
See also Figures S4 and S5.

Please cite this article in press as: Wang et al., BACH1 changes microglial metabolism and affects astrogenesis during mouse brain development, Developmental Cell (2023), https://doi.org/10.1016/j.devcel.2023.11.018

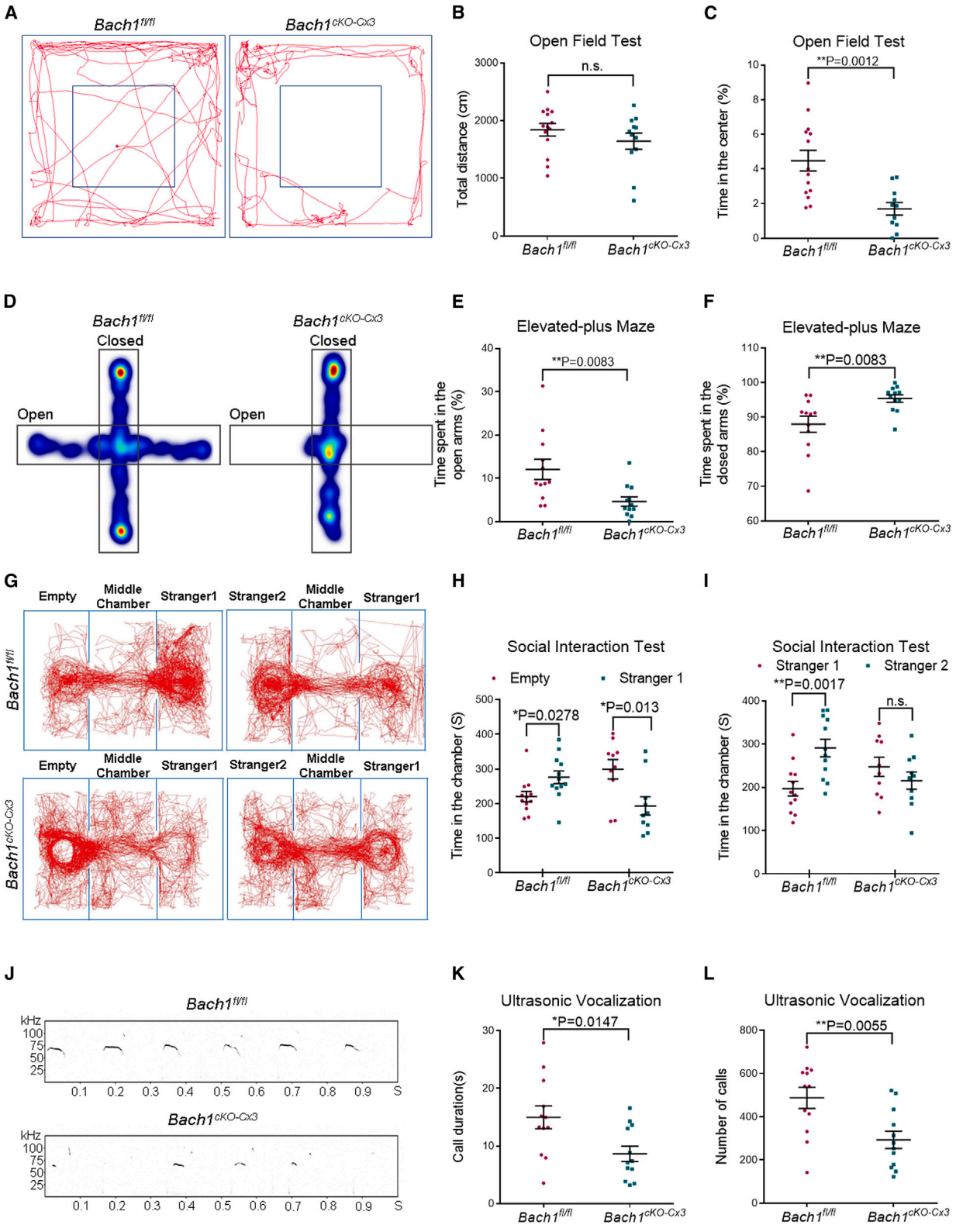

Figure 5. The loss of BACH1 in both adult and pup mice leads to anxiety-like behaviors

(A) Representative motion trajectory images of *Bach1*$^{fl/fl}$ and *Bach1*$^{cKO\text{-}Cx3}$ mice in open field test. The outer box represents the total zone, and the inner box represents the central zone.

(B) The total moving distance was not different between *Bach1*$^{fl/fl}$ and *Bach1*$^{cKO\text{-}Cx3}$ mice within 5 min.

(legend continued on next page)

Please cite this article in press as: Wang et al., BACH1 changes microglial metabolism and affects astrogenesis during mouse brain development, Developmental Cell (2023), https://doi.org/10.1016/j.devcel.2023.11.018

Quantitative analysis showed that CD45+CD11b+ cells were reduced in the mutant cerebral cortex (Figure S7G). Gene ontology (GO) analysis exhibited that the downregulated and the upregulated genes were significantly enriched in terms related to cell proliferation and astrocyte differentiation (Figures 6H and 6I). In addition, 8 significantly different genes were screened based on the results of GO analysis and verified by real-time PCR (Figures 6J and 6K). *Lrrc15* has been shown to be involved in tumor immunity, but its possible function in cortical development has not been reported.[33] Moreover, volcano maps showed differentially expressed genes in *Bach1*$^{fl/fl}$ and *Bach1*$^{cKO\text{-}Cx3}$ mice (Figures 6L and 6M). Enzyme-linked immunosorbent assay (ELISA) and western blotting confirmed that LRRC15 was significantly reduced in *Bach1*-deficient microglia (Figures S7H–S7J). Rotenone drives mitochondrial complex 1 to uncouple from the electron transport chain (ETC) and produce adenosine 5′-triphosphate through glycolysis, leading to lactate accumulation. Our study found that the expression of LRRC15 in microglia treated with rotenone increased synchronously with that of Pan-lysine lactylation (Figures S7K and S7L). Furthermore, to determine whether H4K12la is a specific lactate modification site regulating the expression of LRRC15 in microglia, ChIP analysis showed that H4K12la enrichment in the *Lrrc15* promoter region was decreased in *Bach1*$^{cKO\text{-}Cx3}$ microglia (Figure S7M). Notably, we found that both H4K12la and LRRC15 levels were reduced after treatment with C646, an inhibitor of acetyltransferase P300, but the lactate modification and LRRC15 levels were not affected by treatment with trichostatin A (TSA), an inhibitor of histone deacetylase (HDAC) (Figures S7N and S7O). Taken together, these results suggest that decreased lactate production by *Bach1*-deficient microglia weakens LRRC15 expression through H4K12la.

LRRC15 participates in astrogenesis through the CD248-JAK-STAT3 signal transduction and rescues BACH1-depletion defects

To explore the molecular mechanism of dysfunctional astrogenesis caused by *Bach1*-deleted microglia, we executed the Kyoto Encyclopedia of Genes and Genomes (KEGG) pathway analysis on RNA-seq dataset and identified potential responses involving ligand-receptor interaction in mutational microglia (Figure 7A). Previous research has displayed that CD248 is co-expressed with LRRC15 in the tumor microenvironment and may act as an unknown receptor for LRRC15.[34] Therefore, we detected *Cd248* mRNA levels in astrocyte, NPCs, neurons, and microglia, and we found that *Cd248* was highly expressed in astrocyte (Figure 7B). Immunofluorescence staining showed that LRRC15 was localized to microglia cell membrane (Figure 7C). Furthermore, we found that HA-tagged LRRC15 pulled down FLAG-tagged CD248 and that FLAG-tagged CD248 similarly pulled down HA-tagged LRRC15 through co-immunoprecipitation (coIP) assays (Figures 7D and 7E), indicating that there was a direct interaction between LRRC15 and CD248. In addition, we visualized this interaction in N2a cells and found that LRRC15 co-expressed with CD248 in the cell membrane (Figure 7F). Furthermore, considering that the JAK/STAT3 pathway is a classical signaling pathway that regulates the expression of genes related to astrogenesis, we detected decreased levels of p-JAK1/2 and p-STAT3 in astrocyte progenitors of *Bach1*$^{cKO\text{-}Cx3}$ mice (Figures 7G–7I). We also examined whether CD248 forms signal transduction complexes with other signal transduction subunits by coIP assays, such as glycoprotein 130 (GP130). The results displayed that there was a direct interaction between CD248 and GP130 (Figures 7J and 7K). Together, these results determined that the microglia-derived LRRC15 regulates astrogenesis by interacting with the CD248 to activate the GP130-JAK-STAT3 pathway. To explore whether exogenous LRRC15 could rescue the developmental disorder caused by microglial *Bach1* deficiency, we introduced LRRC15 into the astrogenesis process *in vitro*. Briefly, primary microglia and glial progenitors were co-cultured with LRRC15 (Figure 7L). We evaluated the proportion of BLBP+ and GFAP+ cells and found that the number of BLBP+ and GFAP+ cells in the *Bach1*$^{cKO\text{-}Cx3}$ group increased to that in the *Bach1*$^{fl/fl}$ group treated with LRRC15 (Figures 7M and 7N). Taken together, our study provided insights into the regulation of astrogenesis by microglial metabolism during brain development and focused on a specific downstream molecule, *Lrrc15*, which interacts with CD248 to trigger the GP130-JAK-STAT3 pathway.

DISCUSSION

During early brain development, multiple systems work together to ensure the orderly assembly of the cerebral cortex. One of the fundamental problems to be solved is how the

(C) The time spent in the center zone was decreased in *Bach1*$^{cKO\text{-}Cx3}$ mice within 5 min.
(D) Representative tracks of *Bach1*$^{fl/fl}$ and *Bach1*$^{cKO\text{-}Cx3}$ mice in the elevated-plus maze test.
(E) The time spent in the open arms was reduced in *Bach1*$^{cKO\text{-}Cx3}$ mice.
(F) The time spent in the closed arms was increased in *Bach1*$^{cKO\text{-}Cx3}$ mice.
(G) Representative motion trajectory images of *Bach1*$^{fl/fl}$ and *Bach1*$^{cKO\text{-}Cx3}$ mice in social interaction test. Representative trajectory on the left is from "stranger 1-empty" in the sociability session. Representative trajectory on the right is from "stranger 1-stranger 2" in the social novelty preference session.
(H) In the social interaction session, statistical analysis showed that *Bach1*$^{cKO\text{-}Cx3}$ mice spent less time in the right chamber containing strange and more time in the left empty chamber.
(I) In the social novelty preference session, statistical analysis exhibited that *Bach1*$^{cKO\text{-}Cx3}$ spent more time in the right chamber containing stranger 1 and did not present a significant preference for the left chamber containing stranger 2.
(J) Representative spectrogram of the ultrasonic vocalizations (USVs) in isolated pups at P8.
(K and L) Statistical analysis showed that the call duration (K) and number (L) of *Bach1*$^{cKO\text{-}Cx3}$ pups were decreased at P8 (for *Bach1*$^{fl/fl}$ mice, n = 12–14; for *Bach1*$^{cKO\text{-}Cx3}$ mice, n = 10–12).
All data are presented as the mean ± SEM. Unpaired two-tailed Student's t test or one-way ANOVA; *p < 0.05, **p < 0.01, ***p < 0.001, ****p < 0.0001, n.s., not significant.
See also Figure S6.

Please cite this article in press as: Wang et al., BACH1 changes microglial metabolism and affects astrogenesis during mouse brain development, Developmental Cell (2023), https://doi.org/10.1016/j.devcel.2023.11.018

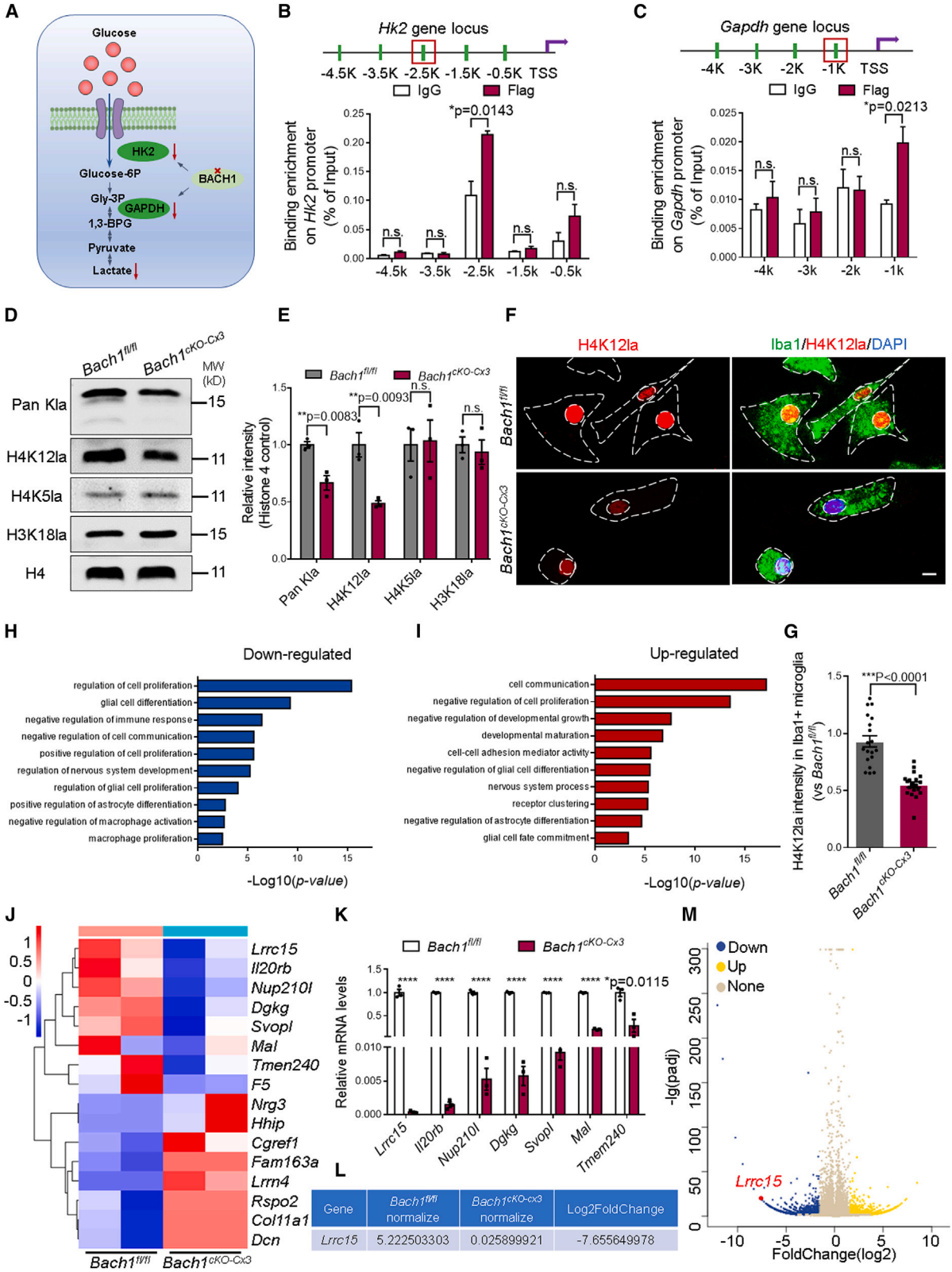

(legend on next page)

Please cite this article in press as: Wang et al., BACH1 changes microglial metabolism and affects astrogenesis during mouse brain development, Developmental Cell (2023), https://doi.org/10.1016/j.devcel.2023.11.018

various systems achieve precise self-regulation and mutual communication. Microglia are highly heterogeneous in order to maintain homeostasis and coordinate the development of other systems, among which the metabolic homeostasis in the embryonic development of microglia has been concerned.[11] Most recent research on astrocytes has focused on their role in the developing and maturing CNS, although less attention has been paid to astrocyte progenitors.[35–38] Our study demonstrated that BACH1 loss in microglia leads to metabolic disorders that reduced lactate modification of microglia-astrocyte progenitors communication mediator. In addition, homeostasis imbalance was also detected in *Bach1*-delected microglia, which we believe may be due to the chain effect caused by the accumulation of certain metabolic intermediates, which is also an interesting issue to be clarified in our subsequent studies. Taken together, our study suggests that microglia constitute an important niche for astrocyte progenitors and participate in the regulation of astrogliosis.

The function of BACH1 in regulating cancer cell metabolism is well known.[39,40] BACH1 suppresses mitochondrial metabolism by inhibiting the expression of mitochondrial ETC complex (I–V) genes and inhibiting pyruvate dehydrogenation activity through pyruvate dehydrogenase kinase regulation.[26] Our results show that the function of *Bach1* is consistent with that in cancer cells, and *Bach1* binds to promoter regions of *Hk2* and *Gadph* to regulate transcription. Combined with RNA-seq, we found that decreased lactate in microglia resulted in decreased lactate modification at H4K12la site of the downstream target *Lrrc15*, thus inhibiting gene transcription.

Astrogenesis in brain development depends on endogenous and peripheral signaling cues in which receptor-ligand interaction is an effective means of communication between different systems.[41–43] The metabolic perturbation of *Bach1*-delected microglia led to a decrease in LRRC15 involved in microglia-astrocyte progenitors cross-talk. Furthermore, we executed coIP tests and found that there was a direct interaction between LRRC15 and CD248 (Figure 7E). Previous studies have shown that the JAK/STAT3 signaling pathway is a classical pathway that regulates the expression of genes related to astrogenesis.[44] Therefore, we examined whether LRRC15 regulates astrogenesis through the JAK/STAT3 signaling pathway. Considering that GP130 is a signal transduction component on the JAK/STAT3 signaling pathway receptor complexes, we executed coIP tests and found that there was a direct interaction between CD248 and GP130 (Figures 7J and 7K). Overall, our data demonstrated that microglia-derived LRRC15 interacted with CD248 to reduce activation of the GP130-JAK/STAT3 pathway. In addition, previous studies have shown that early glial dysplasia can lead to many diseases. Maternal prenatal TLR7 activation reduces the density of Iba1+ microglia in offspring and leads to anxiety-like behaviors.[8] Deletion of uncoupling protein 2 in microglia increases ROS production and abnormal phagocytosis phenotypes and induces anxiety-like behavior.[10] Chimeric mice with astrocyte developmental retardation and morphological abnormalities showed abnormal behaviors, including excessive anxiety and disturbed sleep.[9] These studies suggest that less and activated microglia/less astrocytes in the developing brain are strongly associated with anxiety-like behavior. In our study, *Bach1*$^{cKO\text{-}Cx3}$ mice exhibited anxiety-like behaviors such as impaired exploration ability and social disorder.

In conclusion, our results reveal that signals from metabolic reprogramming of microglia interact with receptors on astrocyte progenitors to regulate astrogenesis during embryonic development. Our study provides insights into microglial metabolic homeostasis, microglia-astrocyte communication, and anxiety-like behaviors.

Limitations of the study

Our study showed that *Bach1*-deficient microglia exhibited dual abnormalities of metabolism and homeostasis, but further studies are needed to clarify whether there is a direct link between metabolic transformation and homeostasis imbalance in *Bach1*-deficient microglia. Although our study shows that there is a reliable receptor-ligand interaction between LRCC15 and CD248, the presence of other ligands in astrocyte progenitors that can interact with LRRC15 requires further investigation.

STAR★METHODS

Detailed methods are provided in the online version of this paper and include the following:

Figure 6. The changing histone lactylation of microglial metabolism damages astrogenesis by targeting LRRC15

(A) The schematic diagram of glycolysis emphasizes that HK2 and GAPDH regulated by BACH.

(B and C) N2a cells were transfected with FLAG-*Bach1* overexpression plasmid and cultured for 3 days before ChIP assay. ChIP experiment verified that *Bach1* binds to the site of the *Hk2* (B) and *Gapdh* (C) promoter (n = 3 independent experiments).

(D and E) Western blotting analysis showing levels of Pan- and site-specific histone lactylation in the cerebral cortex of *Bach1*$^{fl/fl}$ and *Bach1*$^{cKO\text{-}Cx3}$ mice (n = 3 mice per group).

(F and G) Representative confocal images of H4K12la co-stained with Iba1 in microglia of *Bach1*$^{fl/fl}$ and *Bach1*$^{cKO\text{-}Cx3}$ mice (F), with quantification of H4K12la intensity (G) (n = 19 cells per group). Scale bars, 50 μm; for zoom, 10 μm.

(H and I) Gene ontology (GO) analysis of biological processes related to the downregulated (H) and upregulated (I) genes in the microglia of *Bach1*$^{cKO\text{-}Cx3}$ mice at E16.

(J) Heatmap showed that 8 downregulated and 8 upregulated candidate target.

(K) Quantitative real-time PCR showed the expression of *Lrrc15* in microglia was most significantly decreased (n = 3 mice per group).

(L) RNA-seq analysis showing that the *Lrrc15* expression level was dramatically decreased in *Bach1*-delected microglia.

(M) Volcano plots showed the downregulated (blue) and upregulated (yellow) genes in *Bach1*-delected microglia.

All data are presented as the mean ± SEM. Unpaired two-tailed Student's t test or one-way ANOVA; *p < 0.05, **p < 0.01, ***p < 0.001, ****p < 0.0001, n.s., not significant.

See also Figure S7.

Please cite this article in press as: Wang et al., BACH1 changes microglial metabolism and affects astrogenesis during mouse brain development, Developmental Cell (2023), https://doi.org/10.1016/j.devcel.2023.11.018

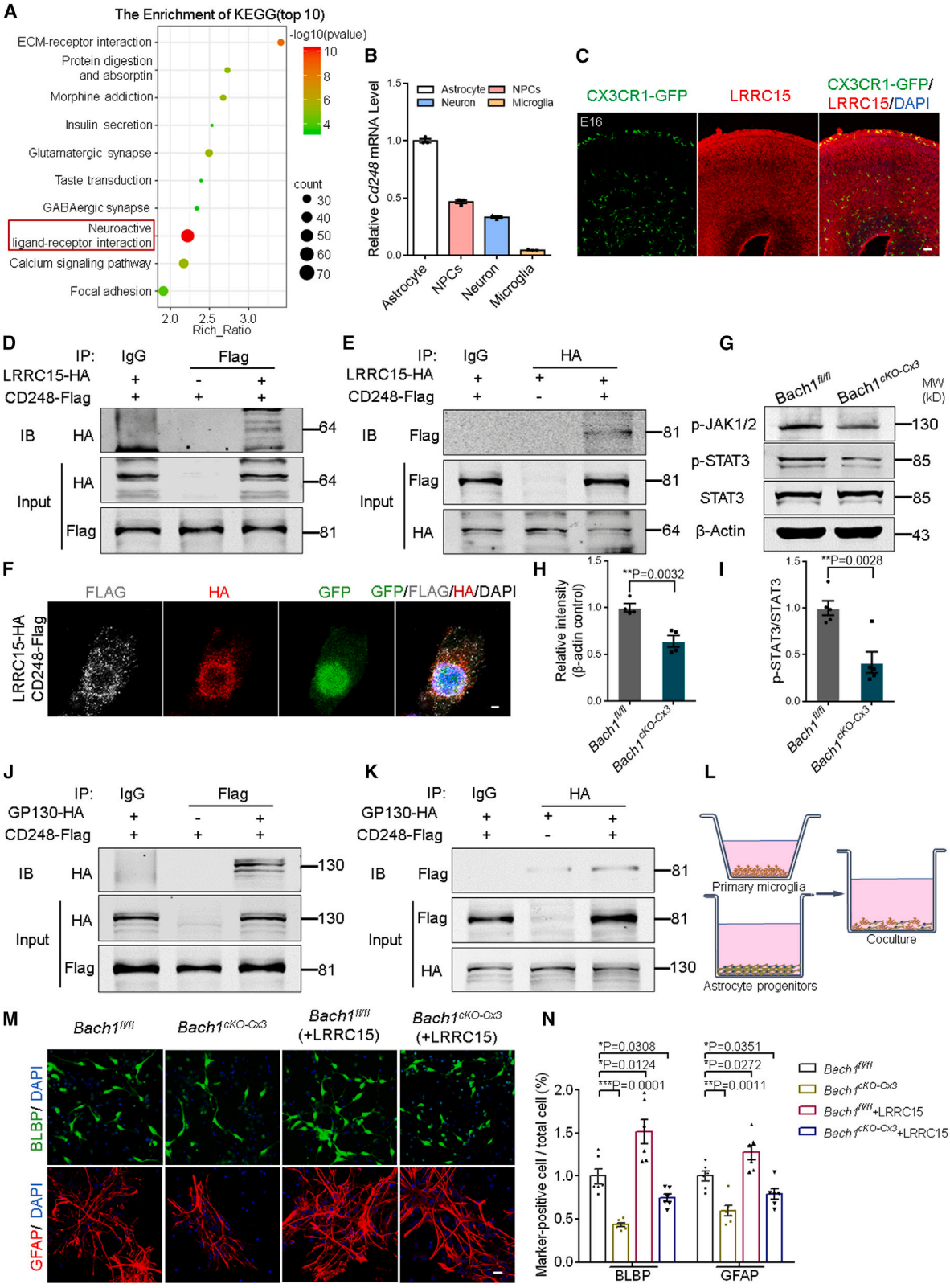

Figure 7. Microglia regulates astrogenesis through CD248-GP130-JAK-STAT signaling pathway in astrocyte progenitors

(A) Representative images of *Bach1*$^{cKO\text{-}Cx3}$ microglia significantly enriched pathway by KEGG pathway analysis. The signaling pathway highlighted by the red rectangle is significantly enriched in *Bach1*$^{cKO\text{-}Cx3}$ microglia.

(legend continued on next page)

SUPPLEMENTAL INFORMATION

Supplemental information can be found online at https://doi.org/10.1016/j.devcel.2023.11.018.

ACKNOWLEDGMENTS

We gratefully thank Zengqiang Yuan (The Brain Science Center, Beijing Institute of Basic Medical Sciences) for providing CX3CR1-GFP mice. This work was supported by grants from the National Natural Science Foundation of China (81825006, 32230040, and 92149304) and the National Key R&D Program of China (2019YFA0110301).

AUTHOR CONTRIBUTIONS

Y.W., W.W., and J.J. conceived the research. Y.W. performed the experiments and drafted the manuscript. W.W. analyzed the data with input from all authors. L.S. and F.J. provided some suggestions on data analysis. M.Z., Y.X., and T.Z. performed the mouse genotype identification experiment. J.J. supervised the project and acquired the funding support.

DECLARATION OF INTERESTS

The authors declare no competing interests.

INCLUSION AND DIVERSITY

We support inclusive, diverse, and equitable conduct of research.

Received: May 2, 2023
Revised: August 22, 2023
Accepted: November 15, 2023
Published: December 14, 2023

REFERENCES

1. Miller, F.D., and Gauthier, A.S. (2007). Timing is everything: making neurons versus glia in the developing cortex. Neuron *54*, 357–369.
2. Nagao, M., Ogata, T., Sawada, Y., and Gotoh, Y. (2016). Zbtb20 promotes astrocytogenesis during neocortical development. Nat. Commun. *7*, 11102.
3. He, F., Ge, W., Martinowich, K., Becker-Catania, S., Coskun, V., Zhu, W., Wu, H., Castro, D., Guillemot, F., Fan, G., et al. (2005). A positive autoregulatory loop of Jak-STAT signaling controls the onset of astrogliogenesis. Nat. Neurosci. *8*, 616–625.
4. Sun, Y., Nadal-Vicens, M., Misono, S., Lin, M.Z., Zubiaga, A., Hua, X., Fan, G., and Greenberg, M.E. (2001). Neurogenin promotes neurogenesis and inhibits glial differentiation by independent mechanisms. Cell *104*, 365–376.
5. Yu, H., Lee, H., Herrmann, A., Buettner, R., and Jove, R. (2014). Revisiting STAT3 signalling in cancer: new and unexpected biological functions. Nat. Rev. Cancer *14*, 736–746.
6. Nakanishi, M., Niidome, T., Matsuda, S., Akaike, A., Kihara, T., and Sugimoto, H. (2007). Microglia-derived interleukin-6 and leukaemia inhibitory factor promote astrocytic differentiation of neural stem/progenitor cells. Eur. J. Neurosci. *25*, 649–658.
7. Matejuk, A., and Ransohoff, R.M. (2020). Crosstalk between astrocytes and microglia: an overview. Front. Immunol. *11*, 1416.
8. Missig, G., Robbins, J.O., Mokler, E.L., McCullough, K.M., Bilbo, S.D., McDougle, C.J., and Carlezon, W.A., Jr. (2020). Sex-dependent

(B) Quantitative real-time PCR assays monitoring expression of *Cd248* in astrocytes, NPCs, neurons, and microglia (n = 3 mice per group).
(C) Immunofluorescence staining of LRRC15 in the cerebral cortex of CX3CR1-GFP mice at E16.
(D and E) 293FT cells were transfected with LRRC15-HA and CD248-FLAG overexpression plasmids for 3 days and harvested for coIP assays.
(F) Immunofluorescence staining of FLAG and HA exhibiting the colocalization of LRRC15 and CD248 in N2a cells. Scale bars, 20 μm.
(G–I) The protein levels of p-JAK1/2 and p-STAT3 in isolated astrocyte progenitors from $Bach1^{fl/fl}$ and $Bach1^{cKO\text{-}Cx3}$ mice were detected (G) and quantified (H and I) by western blotting (for p-JAK1/2, n = 4; for p-STAT3, n = 5).
(J and K) 293FT cells were transfected with GP130-HA and CD248-FLAG overexpression plasmids for 3 days and harvested for coIP assays.
(L) Schematic diagram of microglia and astrocyte progenitors co-culture system.
(M) Immunofluorescence staining image of a microglia-astrocyte progenitors co-culture system with or without LRRC15 (1 ng/mL) stimulation. Microglia and astrocyte progenitors were isolated from $Bach1^{fl/fl}$ and $Bach1^{cKO\text{-}Cx3}$ mice and were co-cultured for BLBP or GFAP staining after 2 and 5 days. Scale bars, 20 μm.
(N) Quantitative analysis of the number of BLBP+ and GFAP+ cells in the co-culture system with or without LRRC15 treatment (n = 6 mice per group).
All data are presented as the mean ± SEM. Unpaired two-tailed Student's t test or one-way ANOVA; *p < 0.05, **p < 0.01, ***p < 0.001, ****p < 0.0001, n.s., not significant.

neurobiological features of prenatal immune activation via TLR7. Mol. Psychiatry *25*, 2330–2341.

9. Windrem, M.S., Osipovitch, M., Liu, Z., Bates, J., Chandler-Militello, D., Zou, L., Munir, J., Schanz, S., McCoy, K., Miller, R.H., et al. (2017). Human iPSC glial mouse chimeras reveal glial contributions to schizophrenia. Cell Stem Cell *21*, 195–208.e6.
10. Yasumoto, Y., Stoiljkovic, M., Kim, J.D., Sestan-Pesa, M., Gao, X.B., Diano, S., and Horvath, T.L. (2021). Ucp2-dependent microglia-neuronal coupling controls ventral hippocampal circuit function and anxiety-like behavior. Mol. Psychiatry *26*, 2740–2752.
11. Li, Y., Li, Z., Yang, M., Wang, F., Zhang, Y., Li, R., Li, Q., Gong, Y., Wang, B., Fan, B., et al. (2022). Decoding the temporal and regional specification of microglia in the developing human brain. Cell Stem Cell *29*, 620–634.e6.
12. Young, A.M.H., Kumasaka, N., Calvert, F., Hammond, T.R., Knights, A., Panousis, N., Park, J.S., Schwartzentruber, J., Liu, J., Kundu, K., et al. (2021). A map of transcriptional heterogeneity and regulatory variation in human microglia. Nat. Genet. *53*, 861–868.
13. Zhang, X., Guo, J., Wei, X., Niu, C., Jia, M., Li, Q., and Meng, D. (2018). Bach1: function, regulation, and involvement in disease. Oxid. Med. Cell. Longev. *2018*, 1347969.
14. Anderson, N.M., and Simon, M.C. (2019). BACH1 orchestrates lung cancer metastasis. Cell *178*, 265–267.
15. Lee, J., Yesilkanal, A.E., Wynne, J.P., Frankenberger, C., Liu, J., Yan, J., Elbaz, M., Rabe, D.C., Rustandy, F.D., Tiwari, P., et al. (2019). Effective breast cancer combination therapy targeting BACH1 and mitochondrial metabolism. Nature *568*, 254–258.
16. Wiel, C., Le Gal, K., Ibrahim, M.X., Jahangir, C.A., Kashif, M., Yao, H., Ziegler, D.V., Xu, X., Ghosh, T., Mondal, T., et al. (2019). BACH1 stabilization by antioxidants stimulates lung cancer metastasis. Cell *178*, 330–345.e22.
17. Yu, X., Chini, C.C., He, M., Mer, G., and Chen, J. (2003). The BRCT domain is a phospho-protein binding domain. Science *302*, 639–642.
18. Liu, T., Wang, Y., Wang, Y., Cheung, S.K., Or, P.M., Wong, C.W., Guan, J., Li, Z., Yang, W., Tu, Y., et al. (2022). The mitotic regulator RCC2 promotes glucose metabolism through BACH1-dependent transcriptional upregulation of hexokinase II in glioma. Cancer Lett. *549*, 215914.
19. Pradhan, P., Vijayan, V., Cirksena, K., Buettner, F.F.R., Igarashi, K., Motterlini, R., Foresti, R., and Immenschuh, S. (2022). Genetic BACH1 deficiency alters mitochondrial function and increases NLRP3 inflammasome activation in mouse macrophages. Redox Biol. *51*, 102265.
20. Zhao, L., Kang, M., Liu, X., Wang, Z., Wang, Y., Chen, H., Liu, W., Liu, S., Li, B., Li, C., et al. (2022). UBR7 inhibits HCC tumorigenesis by targeting Keap1/Nrf2/Bach1/HK2 and glycolysis. J. Exp. Clin. Cancer Res. *41*, 330.
21. Yu, J., Chai, P., Xie, M., Ge, S., Ruan, J., Fan, X., and Jia, R. (2021). Histone lactylation drives oncogenesis by facilitating m(6)A reader protein YTHDF2 expression in ocular melanoma. Genome Biol. *22*, 85.
22. Zhang, D., Tang, Z., Huang, H., Zhou, G., Cui, C., Weng, Y., Liu, W., Kim, S., Lee, S., Perez-Neut, M., et al. (2019). Metabolic regulation of gene expression by histone lactylation. Nature *574*, 575–580.
23. Pan, R.Y., He, L., Zhang, J., Liu, X., Liao, Y., Gao, J., Liao, Y., Yan, Y., Li, Q., Zhou, X., et al. (2022). Positive feedback regulation of microglial glucose metabolism by histone H4 lysine 12 lactylation in Alzheimer's disease. Cell Metab. *34*, 634–648.e6.
24. Vay, S.U., Flitsch, L.J., Rabenstein, M., Rogall, R., Blaschke, S., Kleinhaus, J., Reinert, N., Bach, A., Fink, G.R., Schroeter, M., et al. (2018). The plasticity of primary microglia and their multifaceted effects on endogenous neural stem cells in vitro and in vivo. J. Neuroinflammation *15*, 226.
25. Liu, L.R., Liu, J.C., Bao, J.S., Bai, Q.Q., and Wang, G.Q. (2020). Interaction of microglia and astrocytes in the neurovascular unit. Front. Immunol. *11*, 1024.
26. Padilla, J., and Lee, J. (2021). A novel therapeutic. Target, Bach1, regulates cancer metabolism. Cells *10*, 634.
27. Bélanger, M., Allaman, I., and Magistretti, P.J. (2011). Brain energy metabolism: focus on astrocyte-neuron metabolic cooperation. Cell Metab. *14*, 724–738.
28. Bonvento, G., and Bolaños, J.P. (2021). Astrocyte-neuron metabolic cooperation shapes brain activity. Cell Metab. *33*, 1546–1564.
29. Ioannou, M.S., Jackson, J., Sheu, S.H., Chang, C.L., Weigel, A.V., Liu, H., Pasolli, H.A., Xu, C.S., Pang, S., Matthies, D., et al. (2019). Neuron-astrocyte metabolic coupling protects against activity-induced fatty acid toxicity. Cell *177*, 1522–1535.e14.
30. He, D., Xu, H., Zhang, H., Tang, R., Lan, Y., Xing, R., Li, S., Christian, E., Hou, Y., Lorello, P., et al. (2022). Disruption of the IL-33-ST2-AKT signaling axis impairs neurodevelopment by inhibiting microglial metabolic adaptation and phagocytic function. Immunity *55*, 159–173.e9.
31. Lehrman, E.K., Wilton, D.K., Litvina, E.Y., Welsh, C.A., Chang, S.T., Frouin, A., Walker, A.J., Heller, M.D., Umemori, H., Chen, C., and Stevens, B. (2018). CD47 protects synapses from excess microglia-mediated pruning during development. Neuron *100*, 120–134.e6.
32. Vainchtein, I.D., Chin, G., Cho, F.S., Kelley, K.W., Miller, J.G., Chien, E.C., Liddelow, S.A., Nguyen, P.T., Nakao-Inoue, H., Dorman, L.C., et al. (2018). Astrocyte-derived interleukin-33 promotes microglial synapse engulfment and neural circuit development. Science *359*, 1269–1273.
33. Krishnamurty, A.T., Shyer, J.A., Thai, M., Gandham, V., Buechler, M.B., Yang, Y.A., Pradhan, R.N., Wang, A.W., Sanchez, P.L., Qu, Y., et al. (2022). LRRC15(+) myofibroblasts dictate the stromal setpoint to suppress tumour immunity. Nature *611*, 148–154.
34. Cao, S., Peterson, S.M., Müller, S., Reichelt, M., McRoberts Amador, C., and Martinez-Martin, N. (2021). A membrane protein display platform for receptor interactome discovery. Proc. Natl. Acad. Sci. USA *118*, e2025451118.
35. Qian, X., Shen, Q., Goderie, S.K., He, W., Capela, A., Davis, A.A., and Temple, S. (2000). Timing of CNS cell generation: a programmed sequence of neuron and glial cell production from isolated murine cortical stem cells. Neuron *28*, 69–80.
36. Cheng, Y.T., Woo, J., Luna-Figueroa, E., Maleki, E., Harmanci, A.S., and Deneen, B. (2023). Social deprivation induces astrocytic TRPA1-GABA suppression of hippocampal circuits. Neuron *111*, 1301–1315.e5.
37. Endo, F., Kasai, A., Soto, J.S., Yu, X., Qu, Z., Hashimoto, H., Gradinaru, V., Kawaguchi, R., and Khakh, B.S. (2022). Molecular basis of astrocyte diversity and morphology across the CNS in health and disease. Science *378*, eadc9020.
38. Takano, T., Wallace, J.T., Baldwin, K.T., Purkey, A.M., Uezu, A., Courtland, J.L., Soderblom, E.J., Shimogori, T., Maness, P.F., Eroglu, C., and Soderling, S.H. (2020). Chemico-genetic discovery of astrocytic control of inhibition in vivo. Nature *588*, 296–302.
39. Hayes, J.D., Dinkova-Kostova, A.T., and Tew, K.D. (2020). Oxidative Stress in cancer. Cancer Cell *38*, 167–197.
40. Sato, M., Matsumoto, M., Saiki, Y., Alam, M., Nishizawa, H., Rokugo, M., Brydun, A., Yamada, S., Kaneko, M.K., Funayama, R., et al. (2020). BACH1 promotes pancreatic cancer metastasis by repressing epithelial genes and enhancing epithelial-mesenchymal transition. Cancer Res. *80*, 1279–1292.
41. Pellegrino, G., Martin, M., Allet, C., Lhomme, T., Geller, S., Franssen, D., Mansuy, V., Manfredi-Lozano, M., Coutteau-Robles, A., Delli, V., et al. (2021). GnRH neurons recruit astrocytes in infancy to facilitate network integration and sexual maturation. Nat. Neurosci. *24*, 1660–1672.
42. Sardi, S.P., Murtie, J., Koirala, S., Patten, B.A., and Corfas, G. (2006). Presenilin-dependent ErbB4 nuclear signaling regulates the timing of astrogenesis in the developing brain. Cell *127*, 185–197.

43. Shinmyo, Y., Saito, K., Hamabe-Horiike, T., Kameya, N., Ando, A., Kawasaki, K., Duong, T.A.D., Sakashita, M., Roboon, J., Hattori, T., et al. (2022). Localized astrogenesis regulates gyrification of the cerebral cortex. Sci. Adv. *8*, eabi5209.

44. Bonni, A., Sun, Y., Nadal-Vicens, M., Bhatt, A., Frank, D.A., Rozovsky, I., Stahl, N., Yancopoulos, G.D., and Greenberg, M.E. (1997). Regulation of gliogenesis in the central nervous system by the JAK-STAT signaling pathway. Science *278*, 477–483.

45. Sirenko, O., Mitlo, T., Hesley, J., Luke, S., Owens, W., and Cromwell, E.F. (2015). High-content assays for characterizing the viability and morphology of 3D cancer spheroid cultures. Assay Drug Dev. Technol. *13*, 402–414.

46. Stoddart, L.A., Vernall, A.J., Denman, J.L., Briddon, S.J., Kellam, B., and Hill, S.J. (2012). Fragment screening at adenosine-A(3) receptors in living cells using a fluorescence-based binding assay. Chem. Biol. *19*, 1105–1115.

Please cite this article in press as: Wang et al., BACH1 changes microglial metabolism and affects astrogenesis during mouse brain development, Developmental Cell (2023), https://doi.org/10.1016/j.devcel.2023.11.018

STAR★METHODS

KEY RESOURCES TABLE

REAGENT or RESOURCE	SOURCE	IDENTIFIER
Antibodies		
Goat anti-IBA1	Abcam	Cat#ab5076; RRID: AB_2224402
Rabbit anti-IBA1	Wako	Cat#019-19741; RRID: AB_839504
Rabbit anti-BLBP	Abcam	Cat#ab32423; RRID: AB_880078
Rabbit anti-BACH1	Abclonal	Cat#A5393; RRID: AB_2766202
Mouse anti-BACH1	Santa Cruz Biotechnology	Cat#sc-271211; RRID: AB_10608972
Rabbit anti-GLAST	Proteintech	Cat#20785-1-AP; RRID: AB_2878738
Rabbit anti-CX3CR1	Abcam	Cat#ab8021; RRID: AB_306203
Rabbit anti-Cleaved caspase3	Cell Signaling Technology	Cat#9664S; RRID: AB_2070042
Rabbit anti-P2Y12/P2RY12	Novus	Cat#NBP2-33870; RRID: AB_2810254
Rat anti Mouse CD68 antibody (clone FA-11)	Bio-Rad	Cat#MCA1957GA; RRID: AB_324217
Rabbit anti-GFAP	Dako	Cat#Z0334; RRID: AB_10013382
Rabbit anti-S100β	Abcam	Cat#ab52642; RRID: AB_882426
Rabbit anti-ALDH1L1	Abcam	Cat#ab56777; RRID: AB_940204
Mouse anti-β-Actin	Proteintech	Cat#60008-1-Ig; RRID: AB_2289225
Rabbit anti-β-Actin	Proteintech	Cat#20536-1-AP; RRID: AB_10700003
Rabbit anti-Flag	Sigma-Aldrich	Cat#F1804; RRID: AB_262044
Rabbit anti-HA	Cell Signaling Technology	Cat#3724S; RRID: AB_1549585
Rabbit anti-IgG	Bioss	Cat#bs-0295p; RRID: AB_3068583
Rabbit anti-Pan Kla	PTM BIO	Cat#PTM-1401; RRID: AB_2868521
Mouse anti-H4K5la	PTM BIO	Cat#PTM-1409;
Rabbit anti-H4K12la	PTM BIO	Cat#PTM-1411;
Rabbit anti-H3K18la	PTM BIO	Cat#PTM-1406RM; RRID: AB_2909438
Mouse anti-p-JAK1/2	Cell Signaling Technology	Cat#66245S; RRID: AB_2799703
Rabbit anti-p-STAT3(Tyr705)	Cell Signaling Technology	Cat#9145S; RRID: AB_2491009
Rabbit anti-STAT3(79D7)	Cell Signaling Technology	Cat#4904S; RRID: AB_331269
Rabbit anti-LRRC15	Abcam	Cat#ab150376;
PE rat anti-mouse CD45 (clone 30-F11)	Biolegend	Cat#103105; RRID: AB_312970
APC rat anti-mouse CD11B (clone M1/70)	eBioscience	Cat#17-0112-83; RRID: AB_469344
Bacterial and virus strains		
pAAV-F4/80-GFP-mir30shRNA (control)	Vigenebio	N/A
pAAV-F4/80-GFP-mir30shRNA (*Bach1*)	Vigenebio	N/A
Chemicals, peptides, and recombinant proteins		
Dulbecco's Modified Eagle Medium (DMEM)	GIBCO	Cat#11995-065
Low Glucose DMEM	GIBCO	Cat#11885-084
DMEMF/12 medium	GIBCO	Cat#11330-032
Neurobasal medium	GIBCO	Cat#21103-049
Fetal Bovine Serum (FBS)	GIBCO	Cat#16000044
Penicillin / Streptomycin	Invitrogen	Cat#15070063
Papain	Worthington	Cat#Ls003119
Poly-D-Lysine	Sigma	Cat#P3655
Laminin	Invitrogen	Cat#23017015
B27 supplement without VA	Invitrogen	Cat#12587010
B27 supplement with VA	Invitrogen	Cat#17504-044
100 × Gluta MAX	Invitrogen	Cat#35050061

(*Continued on next page*)

Please cite this article in press as: Wang et al., BACH1 changes microglial metabolism and affects astrogenesis during mouse brain development, Developmental Cell (2023), https://doi.org/10.1016/j.devcel.2023.11.018

Continued

REAGENT or RESOURCE	SOURCE	IDENTIFIER
MEM Non-Essential Amino Acids Solution	GIBCO	Cat#11140050
EGF	Invitrogen	Cat#PHG0311
bFGF	Invitrogen	Cat#PHG0026
DPBS	GIBCO	Cat#C14190500CP
GenEscort I	Wisegen	Cat#WIS 1100
Lipo plus	SAGECREATION	Cat#Q03003
Polybrene	Sigma-Aldrich	Cat#TR-1003-G
7-AAD	Biolegend	Cat#420404
RIPA Lysis buffer	Solarbio	Cat#R0010
Co-IP Lysis buffer	Beyotime Biotechnology	Cat#P0013
TRIzol	Ambion Life Technolog	Cat#15596018
L-Lactate	MedChemExpress	Cat#HY-P2807
MitoTracker	ThermoFisher Scientific	Cat#M22426
Anti-HA-tag magnetic beads	MBL	Cat#M132-11
Anti-flag-tag magnetic beads	MBL	Cat#M185-11
Anti-IgG beads	Invitrogen	Cat#10004D
Biotinylated Mouse LRRC15 / LIB Protein	ACROBiosystems	Cat#LR5-M82E6
DAPI	ThermoFisher Scientific	Cat#D3571
Critical commercial assays		
Fast Quant RT Kit	TIANGEN	Cat#KR106-02
SuperReal PreMix Plus (SYBR Green) PCR Kit	TIANGEN	Cat#FP205-02
TIANamp Genomic DNA Kit	TIANGEN	Cat#DP304-03
Mitochondrial Membrane Potential Assay Kit with TMRE	Beyotime Biotechnology	Cat#C2001S
L-LA Assay Kit	Solarbio	Cat#BC2235
RNAprep Pure Micro Kit	TIANGEN	Cat#DP420
Mouse Leucine-rich repeat-containing protein 15 (LRRC15) ELISA Kit	Abebio	Cat#AE35142MO
Deposited data		
Raw and analyzed data of bulk RNA-seq	This paper	GEO: GSE227957
Experimental models: Cell lines		
HEK293 Cell Line	ATCC	ATCC CRL-1573; RRID: CVCL_0045
Mouse neuroblastoma N2a	ATCC	ATCC CCL-131; RRID: CVCL_0470
Experimental models: Organisms/strains		
Mouse: *Bach1*$^{fl/fl}$	Shanghai Model Organsms Center	N/A
Mouse: *Cx3cr1*-cre	Jackson Laboratory	Stock No: 025524
Mouse: *Cx3cr1-GFP*	Jackson Laboratory	Stock No: 005582
Mouse: *hGfap*-cre	Jackson Laboratory	Stock No: 004600
Oligonucleotides		
See Table S1 for primers used in the study	This paper	N/A
Recombinant DNA		
pSicoR-GFP	Addgene	N/A
pSicoR-GFP- *Bach1-shRNA1*: GCGTACACAATATCGAGGAAT	This paper	N/A
pSicoR-GFP- *Bach1-shRNA1*: GCTCGACTGTATCCATGACAT	This paper	N/A
PCDH	System Biosciences	Cat#CD511B-1
PCDH-3flag-*Bach1*	This paper	N/A
PCDH-3flag-*Lrrc15*	This paper	N/A

(*Continued on next page*)

Please cite this article in press as: Wang et al., BACH1 changes microglial metabolism and affects astrogenesis during mouse brain development, Developmental Cell (2023), https://doi.org/10.1016/j.devcel.2023.11.018

Continued

REAGENT or RESOURCE	SOURCE	IDENTIFIER
PCDH-3HA-*Lrrc15*	This paper	N/A
PCDH-3flag-*Cd248*	This paper	N/A
PCDH-3HA-*Cd248*	This paper	N/A
PCDH-3flag-*Gp130*	This paper	N/A
PCDH-3HA-*Gp130*	This paper	N/A
Software and algorithms		
Zen Microscope software	Zeiss	https://www.zeiss.com/microscopy/int/products/microscope-software/zen.html
ImageXpress High Content Confocal Imaging System	Molecular Devices	https://www.moleculardevices.com/products/cellular-imaging-systems/high-content-imaging/imagexpress-micro-confocal#gref
LI-COR Image Studio Software	LI-COR Biosciences	https://www.licor.com/bio/products/software/image_studio/?gclid=EAIaIQobChMIrv7s26ug1wIVQUCGCh1kvQgLEAAYASAAEgLcYPD_BwE
Avisoft RECORDER USGH	Avisoft Bioacoustics	https://www.avisoft.com/downloads/
Avisoft SASLab Pro	Avisoft Bioacoustics	https://www.avisoft.com/downloads/
ABI7500 real-time PCR system	Applied Biosystems	https://www.thermofisher.com/us/en/home/life-science/pcr/real-time-pcr/real-time-pcr-instruments/7500-fast-real-time-pcr-system.html
Imaris 9.7	Imaris	http://www.bitplane.com/imaris/imaris
GraphPad Prism 6.0	GraphPad	https://www.graphpad.com/
Seahorse Wave	Agilent	http://www.agilent.com/en-us/products/cell-analysis-(seahorse)/software-download-for-wave-desktop
FlowJo	FlowJo 10.8.1	https://www.flowjo.com/solutions/flowjo

RESOURCE AVAILABILITY

Lead contact

Further information and requests for resources and reagents should be directed to and will be fulfilled by the lead contact, Jianwei Jiao (jwjiao@ioz.ac.cn).

Materials availability

Plasmids and the antibody generated in this study will be shared by the lead contact upon request.

Data and code availability

Sequencing data has been deposited on the Gene Expression Omnibus website with accession number GSE227957.

This paper does not report original code.

Any additional information required to reanalyze the data reported in this work paper is available from the lead contact upon request.

EXPERIMENTAL MODEL AND STUDY PARTICIPANT DETAILS

Animals

The Institute of Cancer Research (ICR) pregnant mice for in utero electroporation were provided by Vital River. *Cx3cr1*-Cre mice (JAX stock # 025524: B6J.B6N(Cg)-Cx3cr1$^{tm1.1(cre)Jung}$/J) and *Cx3cr1-GFP* mice (JAX stock # 005582: B6.129P2(Cg)-Cx3cr1^{tm1Litt}/J) were purchased from the Jackson Laboratory. *Bach1*$^{fl/fl}$ mice were purchased from Shanghai model organisms. *Bach1*$^{cKO\text{-}Cx3}$ and *Bach1*$^{cKO\text{-}Gfap}$ mice were generated by crossing *Bach1*$^{fl/fl}$ mice with *Cx3cr1*-Cre and *hGfap*-Cre mice. All mice were housed on a 12h light/dark cycle. All animal feeding and experiments were approved by the Experiment Animal Center of Institute of Zoology, Chinese Academy of Sciences (IOZ20190080). Exact age of the mice are listed in Table S2.

Please cite this article in press as: Wang et al., BACH1 changes microglial metabolism and affects astrogenesis during mouse brain development, Developmental Cell (2023), https://doi.org/10.1016/j.devcel.2023.11.018

Cell cultures

Human embryonic kidney 293T cells (ATCC, CRL-1573) and mouse neuroblastoma N2a (ATCC CCL-131) cells were cultured in high glucose Dulbecco's Modified Eagle Medium (DMEM) (Gibco, 11995-065) supplemented with 10% fetal bovine serum (FBS) (Gibco,16000044) and 1% penicillin/streptomycin (Invitrogen, 15070063).

For coculture experiments, we first isolated the E16 cerebral cortex into a single-cell suspension (proliferation medium composed of 50% Neurobasal medium (Gibco, 21103-049), 50% DMEMF/12 medium (Gibco, 11330-032), 100× Gluta MAX (Invitrogen, 35050061), 100× penicillin/streptomycin (Invitrogen, 1570063), 50× B27 supplement without VA (Invitrogen, 12587010), 100× MEM Non-Essential Amino Acids Solution (Gibco, 11140050), 10 ng/mL epidermal growth factor (EGF, Invitrogen, PHG0311), and 10 ng/mL basic fibroblast growth factor (bFGF, Invitrogen, PHG0026)) by papain (Worthington, Ls003119) and seeded on a 24-well culture plate pre-coated with 10 μg/ml Poly-d-Lysine (Sigma, P3655) and 5 μg/ml Lamin (Invitrogen, 23017015). At the same time, microglia (microglia were cultured in high glucose Dulbecco's Modified Eagle Medium (DMEM) (Gibco, 11995-065) supplemented with 10% fetal bovine serum (FBS) (Gibco,16000044) and 1% penicillin/streptomycin (Invitrogen, 15070063)) from E16 stage through flow sorting were inoculated on the above 24-well culture plate. The culture medium ratio was 1:1. Immunofluorescence staining BLBP was performed after 2 days of co-culture. In addition, the co-culture system before immunofluorescence staining of GFAP was cultured in proliferation medium for 2 days and then co-cultured in differentiation medium (differentiation medium composed of Low Glucose DMEM (Gibco, 11885-084), 50× B27 supplement without VA (Invitrogen, 12587010), 100× MEM Non-Essential Amino Acids Solution (Gibco, 11140050), 10% fetal bovine serum (FBS) (Gibco, 16000044), 100× penicillin/streptomycin (Invitrogen, 1570063) and 100× Gluta MAX (Invitrogen, 35050061)) for 4 days.

For plasmid transfection, GenEscort I (Wisegen, WIS 1100) was used to transfect 293T cells and Lipo plus (SAGECREATION, Q03003) was used to transfect N2a cells. After 48-72 hours, the cells were harvested for next experiment.

METHOD DETAILS

Plasmid constructs

RNA was extracted from embryonic mouse brain and reversed transcribed with Fast Quant RT Kit (Tian gen). Mouse *Lrrc15* was amplified by PCR and cloned into pCDH-copGFP vector with 3HA-tag. Mouse *Cd248* was amplified by PCR and cloned into pCDH-copGFP vector with 3Flag-tag. The sequences of mouse *Bach1* shRNA1/2 were obtained from Sigma website and cloned into pSicoR-GFP vector. The sequences were listed in Table S1.

Isolation and culture of primary mouse microglia

Primary mice microglia were isolated from neonatal brains (P1-P3). Briefly, cerebral cortices from neonatal brain after removing the meninges were digested into single cells by treatment with 0.25% trypsin at 37°C 10min. The samples were dispersed into a single-cell suspension with a 1 ml pipette before filtering through a 70-μm pore cell strainer (Corning, 352350). Dissociated cells were re-suspended in 15 ml DMEM supplemented with 10% FBS (Gibco,16000044) and 1% penicillin/streptomycin (Invitrogen, 15070063) and seeded in 75 cm^2 culture flasks at 37°C in humidified 5% CO2, 95% air. The confluence of mixed glial cells was basically complete after 7d, and the microglia cells were harvested by shaking at 200 rpm for 4h after 14d.

Lentivirus production and infection

The lentiviral packaged plasmid and core plasmid were transfected into 293T cells using GenEscort I (Wisegen, WIS 1100). The supernatant medium with lentivirus was collected at 48h after transfection, centrifuged at 3000 rpm for 5min, and remove cell debris. For lentivirus infection, half of the primary mouse microglia medium was replaced with virus suspension and 2 μg/mL polybrene (Sigma, TR-1003-G). After 24h, the supernatant medium was changed with new primary mouse microglia medium.

Adeno-associated virus (AAV) injection

To generate the *Bach1* conditional knockdown AAV, shRNAs targeting *Bach1* was inserted into the pAAV-F4/80-GFP-mir30shRNA vector and packaged into the AAV9 virus. pAAV-F4/80-GFP-mir30shRNA (*Bach1*) (titer: 4.47×10^{13} vg/ml) or pAAV-F4/80-GFP-mir30shRNA (control) (titer: 9.91×10^{13} vg/ml) was constructed by Vigene Bioscience (Shandong, China) and injected into the embryonic lateral ventricles through glass micropipette at E13.5. These AAV-injected mice were sacrificed after 2weeks.

Immunostaining

Briefly, brain sections (15 μm or 30 μm) were fixed with 4% paraformaldehyde (PFA) for 30min at room temperature. The brain sections were blocked with 5% bovine serum albumin (BAS) for 1h at room temperature after washing 3 times for 10min with 1% PBST (1% Triton X-100 in 1 M PBS).and then incubated with primary antibodies at 4°C overnight. The cultured cells were fixed with 4% PFA for 20min at room temperature. The cultured cells were blocked with 5% bovine serum albumin (BAS) for 1h at room temperature after washing 3 times for 10min with 0.1% PBST (0.1% Triton X-100 in 1 M PBS), and then incubated with primary antibodies at 4°C overnight. In the following day, the samples were incubated with the fluorescence-labeling second antibodies for 1.5h at room temperature and then captured by Carl Zeiss LSM880 confocal microscope. Secondary antibodies were Alexa Fluor Cy3, Cy5, or 488 (Jackson ImmunoResearch, 1:1000); DAPI (2 mg/ml; Sigma; D9542) was used for nuclear staining.

Please cite this article in press as: Wang et al., BACH1 changes microglial metabolism and affects astrogenesis during mouse brain development, Developmental Cell (2023), https://doi.org/10.1016/j.devcel.2023.11.018

Three-dimensional (3D) reconstruction

Confocal images were acquired from 30-μm Iba1-stained brain sections using a 40× oil objective and a z-stepsize of 0.85 μm. Imaris 9.0 software was used to track Iba1+ microglia from aforementioned 2D confocal images. For each image, 10 cells were randomly selected for tracking. Microglia three-dimensional (3D) reconstruction was described by the "surface" function in Imaris 9.0 software.

Automatic unbiased analysis of microglia morphology

Confocal images were captured using the Molecular Devices ImageXpress High Content Confocal Imaging System as previously described.[45,46] Confocal images were acquired from 30-μm Iba1-stained brain slices using a 40× water objective and a z-stepsize of 1-μm. More than 50 visual fields of 320 x 320 μm size were randomly selected in each brain slice. Image analysis was performed in 2D using 2D Projection (maximum projection) images of confocal image stacks, and these images are uploaded to the analysis platform. The results were exported to Excel and analyzed in GraphPad Prism8.

Seahorse analysis of mitochondrial respiration

The oxygen consumption rate (OCR) and extracellular acidification rate (ECAR) were measured in microglia using an XF Cell Mito Stress kit and Seahorse XFp extracellular flux analyzers (Seahorse Bioscience) according to the manufacturer's protocol. In brief, the flow-sorted microglia were seeded into XF96-well plates (Agilent Technologies, 101085-004) at a density of 10^4 cells/well and incubated overnight. The day of the measurement, cells were automatically exposed to respiratory inhibitor oligomycin (1 μM), FCCP (1 μM), rotenone/antimycin A (0.5 μM) (Seahorse Biosciences) in turn.

TMRE analysis

The TMRE was determined with Mitochondrial Membrane Potential Assay Kit (Beyotime Biotechnology, C2001S) according to the manufacturer's protocol. The whole experiment should be carried out at room temperature. Briefly, the primary mouse microglia were seeded into 24-well plates (costar) at a density of 10^6 cells and left to adhere overnight. Cells cleaned with PBS were incubated in 1× TMRE detection buffer for 20min, and the positive control group was treated with CCCP (10 μm) for 20min before 1× TMRE detection buffer was added. After incubation, the supernatant was removed, washed with preheated cell culture medium twice, and then observed under confocal laser microscope. The maximum excitation wavelength of TMRE is 550 nm and the maximum emission wavelength is 575 nm.

Lactate production analysis

The lactate production was determined with L-LA Assay Kit (Solarbio, BC2235) according to the manufacturer's protocol. Briefly, the flow-sorted microglia were seeded into 24-well plates (costar) at a density of 10^6 cells and left to adhere overnight. Lactate production is quantified by comparison with a standard curve and normalized by cell count and blank.

Quantitative real-time PCR analysis

The total RNA of mouse cerebral cortex or cultured cells was extracted using TRIzol (Invitrogen, 15596018) following the manufacturer's directions, and cDNA was obtained by the FastQuant RT Kit (TIANGEN, KR106-02). Real-time PCR assays were performed using the SuperReal PreMix Plus (SYBR Green I) Kit (TIANGEN, FP205-02) on ABI 7500 real-time PCR system (Applied Biosystems). β-Actin expression used for normalization of real-time PCR reactions. All reactions were repeated at least in three independent biological experiments. Related primer sequences used for real-time PCR were listed in Table S1.

In utero injection

The pregnant ICR mice were anesthetized at E16 by the intraperitoneal injection of 1% tribromoethanol sodium, and the uterine horns were exposed. Recombinant plasmids DNA (>1,500 ng/μl) mixed with eGFP (Venus-GFP) and 0.02% fast green (Sigma) was gently injected into the embryonic lateral ventricles through glass micropipette. Every fetal brain was electroporated with five 50 ms pulses with 950 ms interval at 47 V by using an electroporator (BTX ECM830). Then, the uterine horns were gently returned to abdominal cavity. The electroporated mice were sacrificed at the right time. For mouse postnatal electroporation, 1 ul of recombinant plasmid DNA was gently injected into the lateral ventricles through glass micropipette and three 100 ms pulses with 950-ms interval at 100 V were administered. The electroporated mice were sacrificed at P8. For lactate rescue experiment, 1 μl of lactate (MedChemExpress, HY-P2807, 20 mM) together with 0.02% fast green (Sigma) was injected into the lateral ventricle at E13/E16, and DMSO was used as a control.

Western Blotting and Co-Immunoprecipitation

For western blotting, brain tissues or cells were sonicated in RIPA lysis buffer (Solarbio) containing protease inhibitor cocktail and PMSF. After centrifugation, the protein concentration was measured by Pierce BCA Protein Assay Reagent. Finally, the protein were separated by 12% or 15% SDS-PAGE gel and transferred onto nitrocellulose (NC) membranes. The NC membranes were blocked with 5% skim milk or BSA in PBST (0.05% Tween-20 in 1 M PBS) for 1h at room temperature, and incubated with primary antibodies overnight on shaking table at 4°C. Next day, The bands were visualized and analyzed by the Odyssey (LI-COR Biosciences) software after secondary antibodies for 1.5h at room temperature.

Please cite this article in press as: Wang et al., BACH1 changes microglial metabolism and affects astrogenesis during mouse brain development, Developmental Cell (2023), https://doi.org/10.1016/j.devcel.2023.11.018

For co-immunoprecipitation, cell samples were sonicated in lysis buffer (Beyotime Biotechnology) containing protease inhibitor cocktail and PMSF. The supernatant was incubated with anti-Flag (MBL, M185-11) or HA-tag magnetic beads (MBL, M132-11) overnight at 4°C. The beads were washed 3 times with precold washing buffer and boiled with loading buffer, the supernatant was analyzed by western blot. Secondary antibodies were 800CW Donkey Anti-Mouse IgG (LICOR, 926-32212, 1:1000), 800CW Donkey Anti-Rabbit IgG (LICOR, 926-32213, 1:1000), 680LT Donkey Anti-Mouse IgG (LICOR, 926-68072, 1:1000), and 680LT Donkey Anti-Rabbit IgG (LICOR, 926-68023, 1:1000).

Chromatin immunoprecipitation (ChIP)

Mouse neuroblastoma N2a cells were crosslinked with 1% fresh formaldehyde solution for 15min at room temperature after transfected with Flag tagged *Bach1* overexpression vectors for 48h. Then 2.5 M glycine solution was treated to terminate the crosslinking reaction for 10min at room temperature. Subsequently, these cells washed twice with precold PBS and collected in lysis buffer 1 (50 mM pH 7.5 HEPES–KOH, 140 mM NaCl, 1 mM EDTA, 10% glycerol, 0.5% NP-40, 0.25% Triton X-100, 1% PMSF, 1% cocktail) for 10min at 4°C. After centrifugation at 4000 rpm for 5min at 4°C, the samples were incubated in lysis buffer 2 (200 mM NaCl, 1 mM EDTA, 0.5 mM EGTA, 10 mM pH 8.0 Tris-HCl, 1% PMSF, 1% cocktail) for 12min at 4°C and were sonicated in 650 μl lysis buffer 3 (10 mM pH 8.0 Tris–HCl, 100 mM NaCl, 1 mM EDTA, 0.5 mM EGTA, 0.1% sodium deoxycholate, 0.25% Triton X-100, 1% SDS, 1% PMSF, 1% cocktail) using a sonicator (Scientz-IID) for 20min on ice. The supernatant were incubated with anti-Flag beads (MBL, M185-11) and IgG beads (Invitrogen, 10004D) in Rotational Mixer at 4°C overnight. The IgG beads was incubated with specific antibody (Bioss, bs-0295p) at least 4h before incubation. After the beads were washed three times with low-salt buffer (0.1% SDS, 1% Triton X-100, 2 mM EDTA, 10 mM pH 8.0 Tris-HCl, 150 mM NaCl) and three times with high-salt buffer (0.1% SDS, 1% Triton X-100, 2 mM EDTA, 10 mM pH 8.0 Tris-HCl, 500 mM NaCl), the chromatin complexes were incubated with TES buffer (10mM PH8.0 Tris–HCl, 1mM EDTA, 50mM Nacl) overnight at 65°C. The genomic DNA was extracted by TIANamp Genomic DNA Kit (TIANGEN, DP304-03) and measured by ABI 7500 real-time PCR system (Applied Biosystems). Related primer sequences used for ChIP-qPCR were listed in Table S1.

Enzyme linked immunosorbent assay (ELISA)

For the detection of LRRC15, primary microglia were isolated from the cerebral cortex of P2 neonatal brains and cell samples were collected for ELISA analysis after 2 days of culture. LRRC15 concentrations were quantitatively analyzed by Mouse LRRC15 ELISA Kit (Abebio, AE35142MO) according to the manufacturer's instructions. The absorbance of samples and standards at 450 nm and 570 nm was read by an automatic microplate fluorescence reader and quantitative analysis was calculated by interpolating values into a standard curve which generated from the ELISA kit.

Behavioral tests

The pup mice at P8 were used for Ultrasonic vocalization, and 8-10weeks old $Bach1^{fl/fl}$ or $Bach1^{cKO\text{-}Cx3}$ littermates were used for other behavioral experiments. There were no significant differences between male and female mice in all experimental tests. All behavioral tests were conducted in a quiet environment from 9 am to 4 pm daily. After each mouse was tested, the apparatus was wiped with 75% alcohol to eliminate interference for the next test. EthoVision XT 14.0 was used for data analysis.

Open field test

The 8-10weeks old mice were gently placed into the center of a open filed box (40 cm x 40 cm x 40 cm) and allowed to explore freely for 5min. The software divided the open field into 16 parts and defined the 4 parts in the center as center zone. After that, the total distance and time in the center were recorded and analyzed by Topscan behavioral analysis software for 5min.

Elevated plus maze test

The elevated-plus maze contained two open arms (40 cm x 9.5 cm), two closed arms (40 cm x 9.5 cm x 9.5 cm) and a center area (9.5 cm x 9.5 cm) located 40 cm high above the floor. Mouse were placed gently in the center and the time spent in the open and closed arms were recorded and analyzed by Topscan behavioral analysis software for 5min after 5-min free exploration.

Three-chamber social interaction test

The three-chamber social interaction apparatus contained 3 equally sized chambers (40 cm x 20 cm x 20 cm) with 2 small cages and there was a door (5 cm) between adjacent chambers. The test comprised of three parts. For the first part, after two empty small cages were symmetrically placed in the right and left chambers. tested mice were placed in the middle chamber to habituate the environment for 10min. For the second part, after a stranger-1 mice was placed in right small cage, tested mice were placed in the middle chamber to explore the environment for 10min. For the third part, after a stranger-2 mice was placed in left small cage, tested mice were placed in the middle chamber to explore the environment for 10min. The two stranger mice were the same gender and age. The time spent in each chamber was recorded and analyzed by Topscan behavioral analysis software.

Ultrasonic vocalization (USVs)

The USVs were conducted during 9:00–16:00 as described previously with minor modifications. The pups of $Bach1^{fl/fl}$ or $Bach1^{cKO\text{-}Cx3}$ were isolated individually from their mother and littermates at P8, and placed into a sound attenuating box for 5min. The USVs emission

Please cite this article in press as: Wang et al., BACH1 changes microglial metabolism and affects astrogenesis during mouse brain development, Developmental Cell (2023), https://doi.org/10.1016/j.devcel.2023.11.018

image was visualized on Avisoft Recorder software by Ultra Sound Gate Condenser Microphone CM16 (Avisoft Bioacoustics, Berlin). The microphone was sensitive to a flat frequency response (±6 dB) between 25-140 kHz, and placed 10 cm high above the pups. For acoustical analysis, the original sound data was treated with fast Fourier transform containing 100% frame, Hamming window, 512 FFT length, and 75% time-window overlap. The frequency and time resolution of spectrograms was produced at 488 Hz and 0.512 ms. Call duration and number of calls were recorded and analyed during the test.

Grip strength test

Mice grip strength was performed by a commercial grip strength meter (BioSEB GS3). The mice were placed on the grip strength meter and smoothly pulled back until the grip is released. Each trial was repeated 3 times in succession and the maximum value was selected as the combined forelimb/hindlimb grip strength. Normalize grip strength values by body weight.

Rotarod test

The rotarod test was performed by a rotarod apparatus (Ugo Basile,47750). 5 mice were quickly placed in a separate lane of the rotarod apparatus that accelerates 4–40 rpm for 5min. Latency to fall was recorded by rotarod apparatus. Each mouse was tested twice a day at 4-hour intervals.

Y-maze

The Y-maze apparatus contained three arms with a 120° angle between each neighbor arm. After the three arms were defined as start, old and new arm by software, the mice were put into start arm for 5min free exploration with the new arm closed. After 30min, the mice were put into start arm again for 5min free exploration with the new arm open. The time spent in each arm was recorded and analyzed by Topscan behavioral analysis software.

Marble burying test

The marble burying test contained a standard mouse house cages and 20 black glass marbles (15 mm diameter) which were cleaned by 70% ethanol and dried before use. Before each trial, cages were filled with 5 cm deep fresh bedding with 20 marbles arranged in 4 rows. The test mice were gently placed on the corner of the house cage and allowed to explore freely for 30 minutes. The number of marbles covered by more than two-thirds was counted after the pictures was taken.

Drug administration

Briefly, we prepared two E13 pregnant mice #1 and #2. E13 pregnant mouse (#2) was injected 1 μl of PLX5622 (MedChemExpress, HY-114153, 20 mM) together with 0.02% fast green (Sigma) into the embryonic right ventricle. Two days later, the embryo in the same location of the uterus was injected 1 μl of PLX5622 (MedChemExpress, HY-114153, 20 mM) together with 0.02% fast green (Sigma) into the right ventricle again. Two days later, at E17, 1 μl of PLX5622 (MedChemExpress, HY-114153, 20 mM) together with 0.02% fast green (Sigma) was injected into the right ventricle of the embryo again. Then, 0.1 ug dye (VECTOR Labs, DL-1177-1) together with 0.02% fast green (Sigma) was injected into the left ventricle. #1 Pregnant mice were treated with DMSO as control. After birth, P0 pups with dye were screened. Then, #2 pups were intraperitoneally injected with PLX5622 (MedChemExpress, HY-114153, 50 mg/kg) until P7 every day, and #1 pups were treated with DMSO as a control. In this way, the ablation of microglia is achieved while ensuring the survival of the embryo. The experimental procedure of microglia ablation is shown in Video S1.

RNA-sequencing and data analysis

The E16 cerebral cortex microglia RNA was purified from *Bach1*$^{fl/fl}$ and *Bach1*$^{cKO\text{-}Cx3}$, which is by FACS and RNAprep Pure Micro Kit (TIANGEN, DP420) according to the manufacturer's instructions. Global transcriptome analysis was carried out by Annoroad Genomics. Briefly, the library was constructed after the RNA samples were qualified by Agilent 2100 Bioanalyzer and sequenced by Illumina HiSeq 2500 sequencer. The raw data reported in this paper are accessible in NCBI's GEO (number: GSE227957).

QUANTIFICATION AND STATISTICAL ANALYSIS

All statistical analyses were performed using GraphPad Prism6.0 software and represented as mean ± SEM. Unpaired Two-tailed Student's t tests were used for statistical comparisons between two groups and one-way ANOVA with Tukey's post hoc test was used for multiple comparisons. P-value was considered statistical difference. *P < 0.05, **P < 0.01, ***P < 0.001 and ***P < 0.001, ****P < 0.0001, n.s. means not significant.